Order Number 1333612

Laser spectroscopy of strontium sulfide and alkaline earth monoborohydrides

Pianalto, Frederick Scott, M.S.

The University of Arizona, 1988

U·M·I
300 N. Zeeb Rd.
Ann Arbor, MI 48106

LASER SPECTROSCOPY OF STRONTIUM SULFIDE AND ALKALINE EARTH MONOBOROHYDRIDES

by

Frederick Scott Pianalto

A Thesis Submitted to the Faculty of the

DEPARTMENT OF CHEMISTRY

In Partial Fulfillment of the Requirements
For the Degree of

MASTER OF SCIENCE

In the Graduate College

THE UNIVERSITY OF ARIZONA

1 9 8 8

STATEMENT BY AUTHOR

This thesis has been submitted in partial fulfillment of requirements for an advanced degree at The University of Arizona and is deposited in the University Library to be made available to borrowers under rules of the Library.

Brief quotations from this thesis are allowable without special permission, provided that accurate acknowledgment of source is made. Requests for permission for extended quotation from or reproduction of this manuscript in whole or in part may be granted by the head of the major department or the Dean of the Graduate College when in his or her judgment the proposed use of the material is in the interests of scholarship. In all other instances, however, permission must be obtained from the author.

SIGNED: Frederick Scott Manetto

APPROVAL BY THESIS DIRECTOR

This thesis has been approved on the date shown below:

Peter Bernath — Apr. 4, 1988

P. F. Bernath
Assistant Professor of Chemistry

Date

For Mom, Dad and Grandma McDougal

ACKNOWLEDGMENTS

I wish to express my sincere appreciation to my group members, Leah, Dharshi and Chris. Their patience and support have been invaluable during the last three years.

I wish to respectfully thank my research director, Peter Bernath. His infinite wisdom and generous financial support, which included research assistantships and travel funds, made obtaining my advanced degree both challenging and interesting.

Finally, I want to thank Dr. Keller for his advice and help on diborane preparation methods, and Dr. Smith, Dr. Salzman and Steve Brown for general support.

TABLE OF CONTENTS

LIST OF TABLES

LIST OF FIGURES

ABSTRACT

Three gas phase alkaline earth molecules were analyzed using dye laser spectroscopy.

The $A^1\Sigma^+$ - $X^1\Sigma^+$ transition of gas phase SrS was studied with high resolution techniques. The 0-0, 0-1, 1-1, 2-1, 3-0, 3-2, 4-1, 5-1, and 5-2 bands were rotationally analyzed and spectroscopic constants were determined. The $A^1\Sigma^+$ state was extensively perturbed. Ground state ($X^1\Sigma^+$) constants derived from the analysis of the nine vibrational levels include: ω_e = 388.2643 cm^{-1}, B_e = 0.1208034(33) cm^{-1}, and r_e = 2.439687(14) Å. Excited state ($A^1\Sigma^+$) constants determined include: T_e = 13932.7068(10) cm^{-1}, ω_e = 339.1454(20) cm^{-1}, B_e = 0.1139895(38) cm^{-1}, and r_e = 2.511601(17) Å.

The spectra of calcium and strontium borohydrides were observed using low resolution laser spectroscopy. The spectra were assigned to the $\tilde{A}^2A_1$ - $\tilde{X}^2A_1$ and $\tilde{B}^2E$ - $\tilde{X}^2A_1$ transitions of $CaBH_4$ and $SrBH_4$. The vibrational frequencies of the metal-ligand stretch determined for $CaBH_4$ were 457 cm^{-1} ($\tilde{X}^2A_1$), 473 cm^{-1} ($\tilde{A}^2A_1$), and 465 cm^{-1} ($\tilde{B}^2E$). The corresponding $SrBH_4$ frequencies were 399 cm^{-1}, 420 cm^{-1}, and 421 cm^{-1}.

CHAPTER I

INTRODUCTION

Gas phase spectroscopy has useful applications in interstellar, atmospheric and combustion chemistry. The gas phase offers the distinct advantage, if desired, of a nearly isolated environment. This aspect greatly simplifies the molecular model.

The development of laser techniques has dramatically changed the nature of molecular spectroscopy. Better sensitivity, spectral region coverage and resolution are some of the benefits of the advent of lasers. Free radicals and other short-lived molecules can now be analyzed with relative ease.

Two gas phase laser spectroscopy experiments are presented in this thesis. Chapter II introduces the method of production of gas phase alkaline earth molecules and their analysis with laser techniques. A high resolution rotational analysis of gas phase strontium sulfide (SrS) is discussed in Chapter III. The high resolution techniques provide an easy method for determining precise and accurate molecular parameters, such as bond lengths, rotational constants and vibrational constants. The focus of Chapter IV is a low resolution laser analysis of gas phase calcium and strontium borohydrides. Low resolution techniques give good estimates for electronic transition energies and vibrational frequencies.

This is the first step leading to an in depth, high resolution analysis to determine molecular parameters. Finally, the observed rotational line positions of the SrS $A^1\Sigma^+ - X^1\Sigma^+$ spectrum are presented in Appendix A, and a rotational analysis of a Fourier transform emission spectrum of gas phase BH is presented in Appendix B. This is the first vibration-rotation spectrum recorded for BH. The constants determined are more accurate than those previously reported from an analysis of the ultraviolet spectrum.

Gas phase studies of SrS are rare. The experimental work presented here might be useful for comparisons to the more common CaO and for applications in interstellar chemistry.

Experimental work on gas phase alkali and alkaline earth borohydrides is also rare. However, some theoretical studies are available for the $LiBH_4$ and $NaBH_4$ molecules. Theoreticians have developed a nonrigid model for migration of the cation over a rigid ligand sphere. The alkaline earth borohydride work presented here could offer new insights on this novel molecular behavior.

CHAPTER II

EXPERIMENTAL METHODS

Production of Alkaline Earth Molecules

The molecules of interest were produced and detected in a Broida oven (1). A diagram of the Broida oven and its components is shown in Figure I. To promote the gas phase reaction between an alkaline earth metal vapor and an oxidant vapor, the metal is first vaporized from a resistively heated alumina crucible (A). The vapor is entrained in a carrier gas (B), typically argon, and carried to the reaction region (D). The oxidant vapor is added through the oxidant ring (C), below the reaction region. A reaction between the metal vapor and the oxidant generates the molecular product in the reaction region. Also, the lasers used to excite molecular transitions pass through the reaction region.

The Broida oven is constructed of stainless steel. The chamber contains five access ports. The four ports on the sides of the oven function as follows: 1) vacuum pump attachment, 2) photomultiplier tube attachment (for collecting total fluorescence from the reaction region), 3) quartz window for transmitting light to a monochromator, and 4) quartz window for viewing the reaction region. A fifth access

Figure I. Broida Oven Schematic Diagram (O'Brien, 2).

A: The alkaline earth metal is vaporized in a resistively heated alumina crucible. B: The carrier gas, injected through a metal ring, entrains the alkaline earth vapor and carries it to the reaction region. C: The oxidant is injected below the reaction region. D: The region of the reaction between the metal and the oxidant vapors.

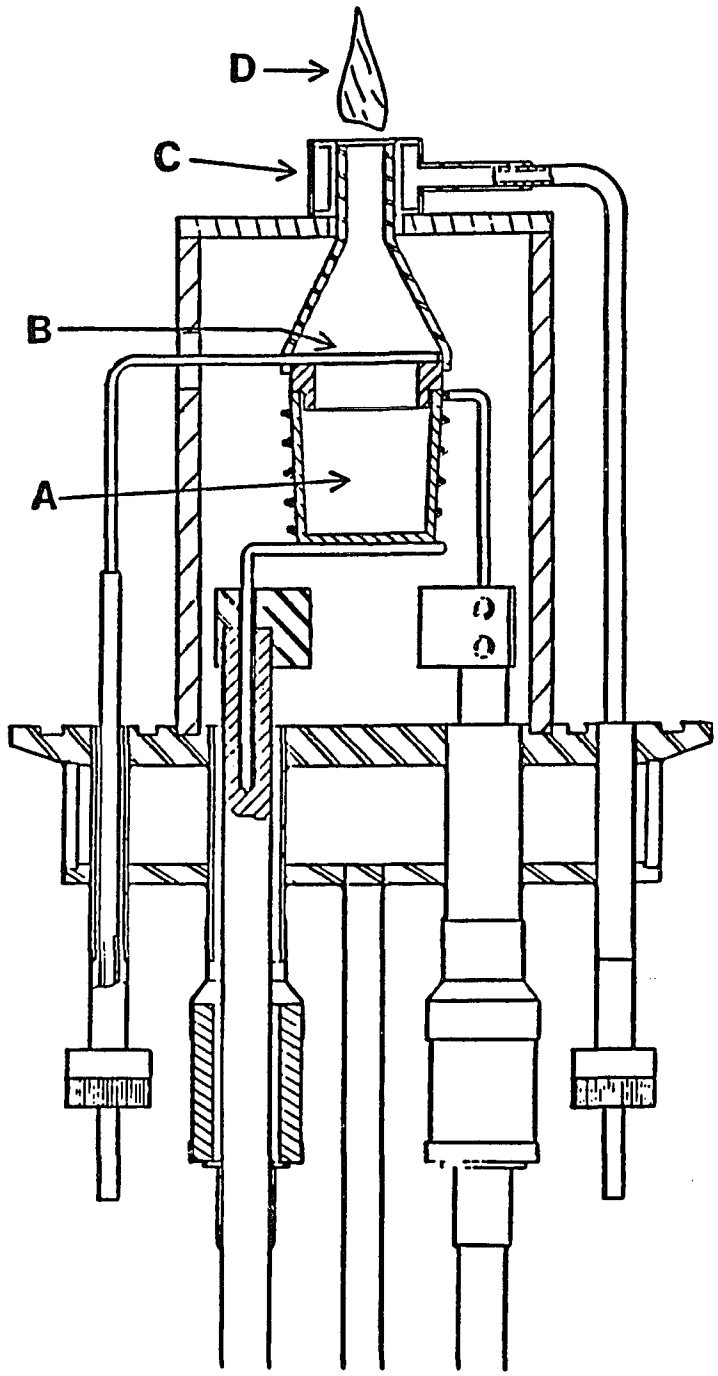
D
C
B
A

port at the top of the oven is a quartz window at Brewster's angle (54° for quartz in the visible region). Here, the laser beams are introduced and directed down through the reaction region.

Total pressures typically maintained inside the oven are about 1-10 Torr, which includes a few millitorr of oxidant. The total and relative pressures of the metal vapor, carrier gas and oxidant often critically determine the success of the experiment.

Low Resolution Laser Experiments

The low resolution experimental apparatus is shown in Figure II. Two methods of low resolution laser analysis are performed: laser excitation experiments and resolved fluorescence experiments.

Laser excitation experiments are performed by scanning the frequency of a Coherent 599-01 dye laser, broadband (1 cm^{-1}), through the molecular frequency region of interest. The dye laser is pumped by a Coherent Innova 90-4 argon ion laser. Total laser induced fluorescence is detected with a photomultiplier tube, and red pass filters placed before the photomultiplier tube are used to remove scattered laser light. The laser excitation experiment is analogous to a classical absorption experiment but detected via laser-induced fluorescence.

Excitation of the alkaline earth metal vapor often enhances (3-5) production of the molecular product, depending upon the oxidant used. To excite the alkaline earth vapor, a second dye laser (Coherent 599-01) is tuned to the $^3P_1$ - $^1S_0$ atomic transition frequency. This laser is spatially overlapped with the laser exciting the molecular transition, and both beams are focussed into the reaction region. The wavelengths for the atomic transitions, 6573 Å for calcium and 6892 Å for strontium, are readily accessible by laser dyes.

Figure II. Experimental Apparatus for Low Resolution Spectra.

The argon ion laser is used to pump the two dye lasers. One dye laser is used to excite the alkaline earth atomic transition in order to promote a reaction between the alkaline earth metal vapor and oxidant vapor. The second dye laser is used to excite the molecular transitions. The two lasers are focussed into the Broida oven. Total laser induced fluorescence from the excited molecular product is either detected directly with a photomultiplier tube (laser excitation spectra), or dispersed with a monochromator followed by detection with a photomultiplier tube (resolved fluorescence spectra). Amplitude modulation techniques, using the chopper and lock-in amplifier, are often employed.

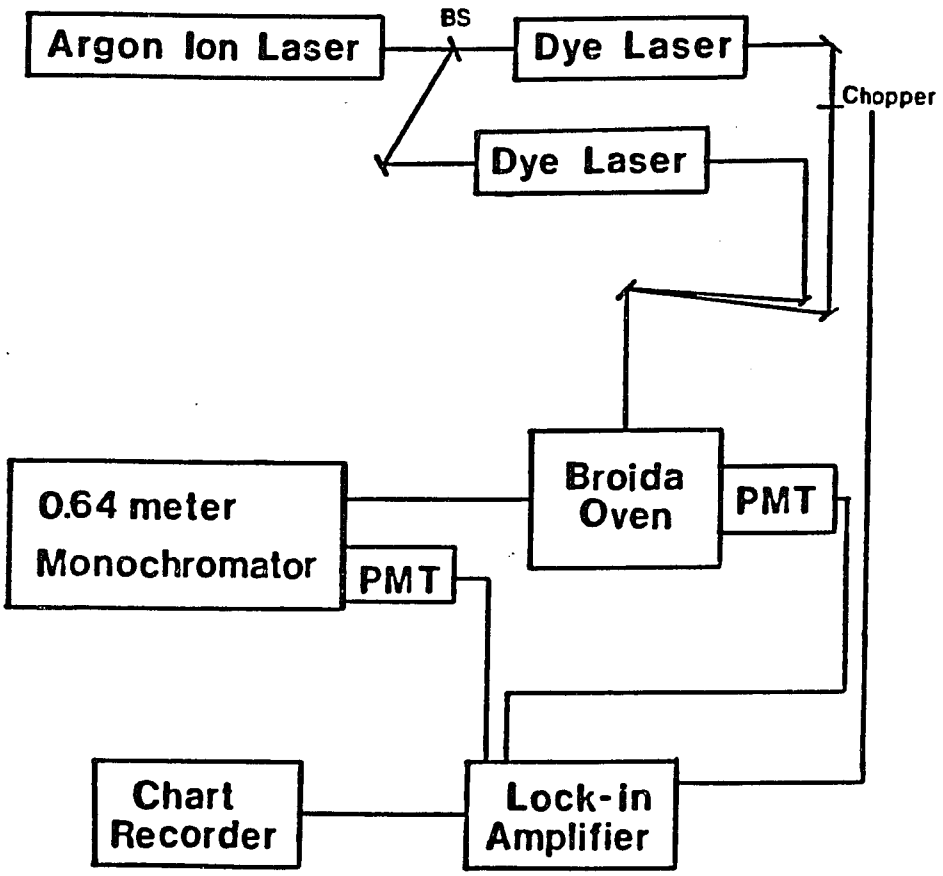
Argon Ion Laser
BS
Dye Laser
Chopper
Dye Laser
Broida Oven
PMT
0.64 meter Monochromator
PMT
Chart Recorder
Lock-in Amplifier

The second type of low resolution experiment, resolved fluorescence, is performed by tuning a dye laser (Coherent 599-01) frequency to a known molecular transition. Emission, or laser induced fluorescence, from the excited molecular state is focussed into a 0.64 m monochromator. The monochromator is scanned to disperse the laser induced fluorescence as a function of wavelength.

Laser excitation experiments, the first type discussed, are usually performed first to determine molecular transition energies. Resolved fluorescence experiments are then performed at the frequency of the molecular transitions to determine vibrational frequencies.

Amplitude modulation methods are often used during low resolution experiments. The laser beam, usually the laser exciting the metal atomic vapor, is modulated with a mechanical chopper, and lock-in detection is used to record the spectrum.

High Resolution Laser Experiments

Low resolution laser techniques are useful for recording electronic and vibrational structure. To record rotational structure in the vibrational bands, high resolution is required. The high resolution experimental apparatus is shown in Figure III.

High resolution spectra are recorded with a computer-controlled Coherent 699-29 Autoscan ring dye laser. The ring dye laser is pumped by a Coherent Innova 20 argon ion laser and has a linewidth of 0.00003 cm^{-1}. The high resolution spectra are Doppler limited, and generally have a linewidth of approximately 1 GHz (0.03 cm^{-1}). The accuracy of the line positions obtained with this system is 0.002 - 0.005 cm^{-1}, depending on the signal to noise ratio of the spectra. Also, if required, a linear (Coherent 599-01) dye laser is used to excite the alkaline earth atomic line.

A 0.64 m monochromator is used as a narrow bandpass filter to select rotational lines of interest. The use of the monochromator in this configuration is often a vital aspect of the experiment, particularily if the high resolution structure is dense. Depending on the placement of the monochromator wavelength, molecular transitions can be detected in connecting branches or bands and away from laser scatter.

Figure III. Experimental Apparatus for High Resolution Spectra.

The two dye lasers are pumped by argon ion lasers. The computer-controlled ring dye laser is used to excite molecular transitions, and the linear dye laser is used to excite the alkaline earth vapor atomic transition. The two dye laser beams are spatially overlapped and focussed into the Broida oven. The monochromator acts as a narrow band-pass filter to disperse the laser induced fluorescence of the molecular product before detection with the photomultiplier tube.

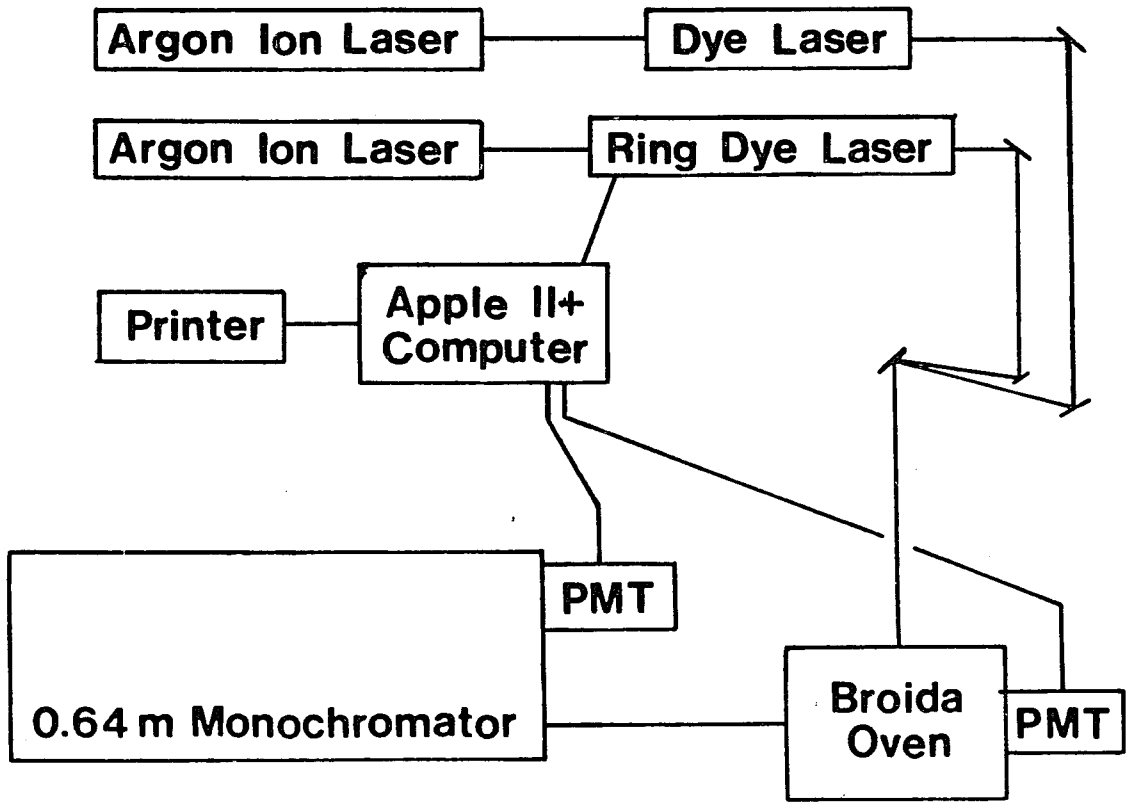
Argon Ion Laser
Dye Laser
Argon Ion Laser
Ring Dye Laser
Printer
Apple II+
Computer
PMT
0.64 m Monochromator
Broida
Oven
PMT

CHAPTER III

STRONTIUM SULFIDE

At one time, alkaline earth oxides and sulfides were of interest as possible candidates for electronic transition chemical lasers (6-7). Also, the compounds are known to exist in many high temperature systems (8-10). Due to the limited amount of spectroscopic data and lack of theoretical calculations on the alkaline earth oxides and sulfides, their electronic states are not well understood.

The only previous work on gas phase strontium sulfide (SrS) is an absorption study by Marcano and Barrow (11) in 1970. The SrS was prepared in a carbon tube furnace at 2000 °C, and the $B^1\Sigma^+ - X^1\Sigma^+$ absorption spectrum in the region of 3600-3900 Å was rotationally analyzed. The $B^1\Sigma^+ - X^1\Sigma^+$ transition energy (T_e) was determined to be 39281.4 cm^{-1}, and extensive perturbations were observed in the $B^1\Sigma^+$ state.

Partridge, Langhoff and Bauschlicher (12) used *ab initio* calculations to determine spectroscopic constants (r_e, ω_e, D_e) for the $X^1\Sigma^+$, $a^3\Pi$ and $A'^1\Pi$ states of the alkaline earth sulfides, including SrS. The transition energies, T_e, for the $a^3\Pi - X^1\Sigma^+$ and $A'^1\Pi - X^1\Sigma^+$ transitions were calculated to be 6870 cm^{-1} and 7179 cm^{-1}, respectively.

Presented here is a rotational analysis of the $A^1\Sigma^+ - X^1\Sigma^+$ system of gas phase SrS using dye laser spectroscopy (13).

The dissociation energy (D_0) of strontium sulfide was determined by Colin, Goldfinger and Jeunehomme (14) and by Marquart and Berkowitz (15) using mass spectrometric techniques. Cater and Johnson (16) used mass spectrometric and vacuum balance effusion techniques to determine a value of 80 ± 4 kcal/mole for D_0, which agrees with the value of Marquart and Berkowitz (15).

Martin and Schaber (17) detected SrS in a low temperature argon matrix using infrared absorption spectroscopy. They observed an absorption at 390 cm^{-1} and tentatively assigned it as the vibrational frequency of SrS.

Electronic transitions for BeS (18-20), MgS (21), CaS (22), and BaS (23-26) have previously been analyzed. In general, the observed excited states were found to be extensively perturbed.

Several states of strontium oxide (SrO) have also been observed. Almkvist and Lagerqvist (27) examined the spectra of SrO from 0.75μ to 1.1μ and observed the $A^1\Sigma^+ - X^1\Sigma^+$ transition with the 0-0 band at 9196 Å. Lagerqvist and Selin (28) further rotationally analyzed bands of the $\Delta v = -2$ sequence and observed an unassigned band sequence in the region of 1.09μ to 1.12μ. Brewer and Hauge (29) have assigned this sequence as $\Delta v = -3$ by comparisons with CaO spectra.

Experimental Details

The strontium sulfide molecule was produced in a Broida oven (1) by the reaction of strontium with carbon disulfide. The strontium metal was vaporized in a resistively heated crucible, carried to the reaction region by argon, and mixed with the oxidant (CS_2). A dye laser, tuned to the ^3P - ^1S strontium atomic transition at 6892.6 Å, was required to promote the reaction. The pressures were approximately 1 Torr argon and a few mTorr carbon disulfide.

Two types of spectra were recorded. Low resolution laser excitation spectra were obtained by scanning a broadband (1 cm^{-1}) CW dye laser and detecting the total fluorescence through a red pass filter with a photomultiplier tube. High resolution (0.003 cm^{-1}) laser excitation spectra were obtained by scanning a computer controlled ring dye laser (Coherent Autoscan 699-29) while detecting fluorescence through a 0.64 m monochromator. The monochromator was used as a narrow bandpass filter to select rotational lines of interest.

The wavemeter of the computer controlled dye laser was calibrated with an iodine cell, and the absolute accuracy of the line positions was approximately ± 0.003 cm^{-1}.

Results and Discussion

A portion of the low resolution laser excitation spectrum of the SrS $A^1\Sigma^+$ - $X^1\Sigma^+$ transition is shown in Figure IV. The spectrum consists of a progression of band sequences. Each individual band exhibits a bandhead degraded to the red, implying a larger bond length in the excited state than in the ground state. The differences in intensity of the vibrational bands is due to laser power variations with frequency as well as Franck-Condon factors. Using the separation between vibrational progressions and sequence structure, the 0-0 band was assigned. The ground state vibrational frequency is about 50 cm^{-1} higher than the excited state frequency, which shows up as changes in the sequence structure separation on either side of the origin (0-0) band.

Following the vibrational assignment, the 0-0, 0-1, 1-1, 2-1, 3-0, 3-2, 4-1, 5-1, and 5-2 bands were recorded at high resolution. 682 rotational lines from the nine bands were recorded. Their frequencies are given in Appendix A. Also, the frequencies of the $A^1\Sigma^+$ - $X^1\Sigma^+$ vibrational bandheads obtained from both low and high resolution spectra are presented in Table I.

The bandhead in the R-branch of the 0-0 band is shown in Figure V. To select out this bandhead, the monochromator was set to detect fluorescence to the $v = 1$ level of the ground ($X^1\Sigma^+$) state.

Figure IV. Low Resolution Spectrum of SrS $A^1\Sigma^+ - X^1\Sigma^+$.

The low resolution SrS laser excitation spectrum consists of a progression of vibrational band sequences. The $\Delta v = 2$, $\Delta v = 1$, and $\Delta v = 0$ sequences are shown, in increasing wavelength. The relative intensities of the bands have not been corrected for the variation in laser power.

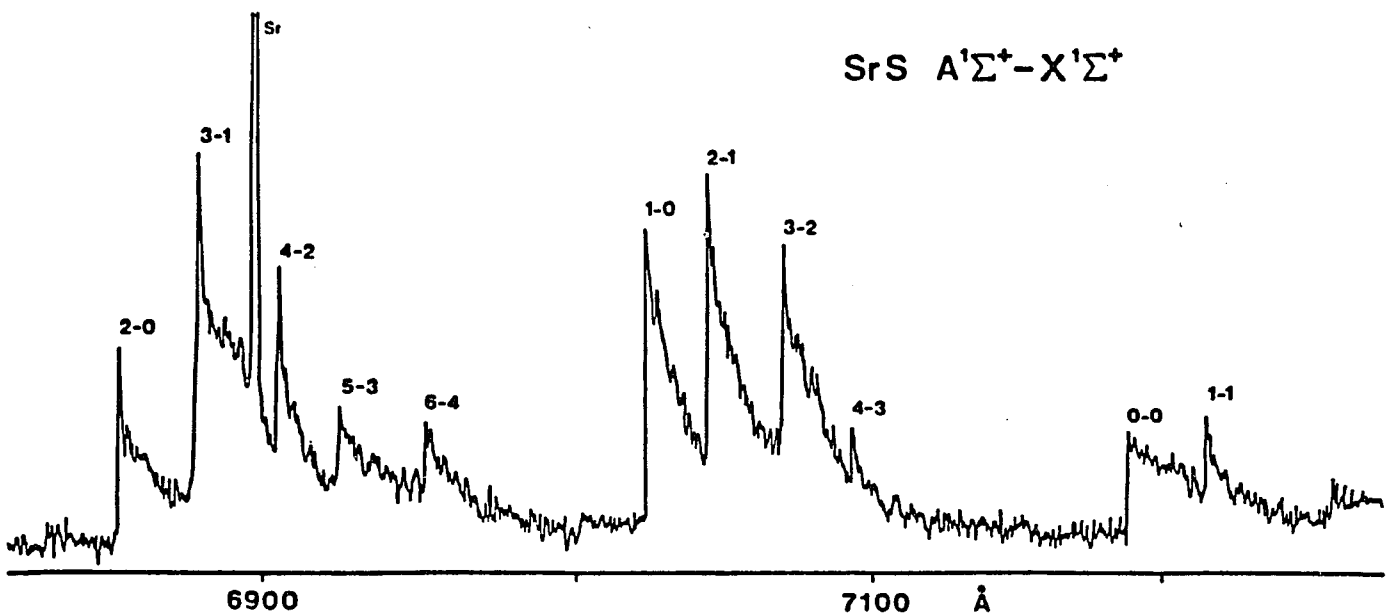
SrS $A^1\Sigma^+ - X^1\Sigma^+$
Sr
2-0
3-1
4-2
5-3
6-4
1-0
2-1
3-2
4-3
0-0
1-1
6900
7100
Å

Table I. Vibrational Bandhead Frequencies for SrS $A^1\Sigma^+ - X^1\Sigma^+$ (in cm^{-1}).

v' \ v''	0	1	2	3
0	13910.3435(50)[a]	13524.7884(50)		
1	14243.8(50)	13862.7019(50)		
2	14594.3(50)	14199.5340(50)		
3	14921.0962(50)	14541.0(50)	14152.4687(50)	
4		14870.0406(50)	14487.3(50)	14103.0(50)
5		15205.0073(50)	14821.9450(50)	14445.9(50)

[a] The number in parenthesis represents one standard deviation uncertainty.

Figure V. High Resolution Spectrum of SrS $A^1\Sigma^+ - X^1\Sigma^+$.

The high resolution spectrum near the R-branch bandhead of the 0-0 band is shown. Rotational lines of high J values coming out of the bandhead are labeled. Low J R-branch lines going into the bandhead are the smaller features. A monochromator was used as a narrow bandpass filter, and its wavelength setting determined the relative intensities of the rotational lines.

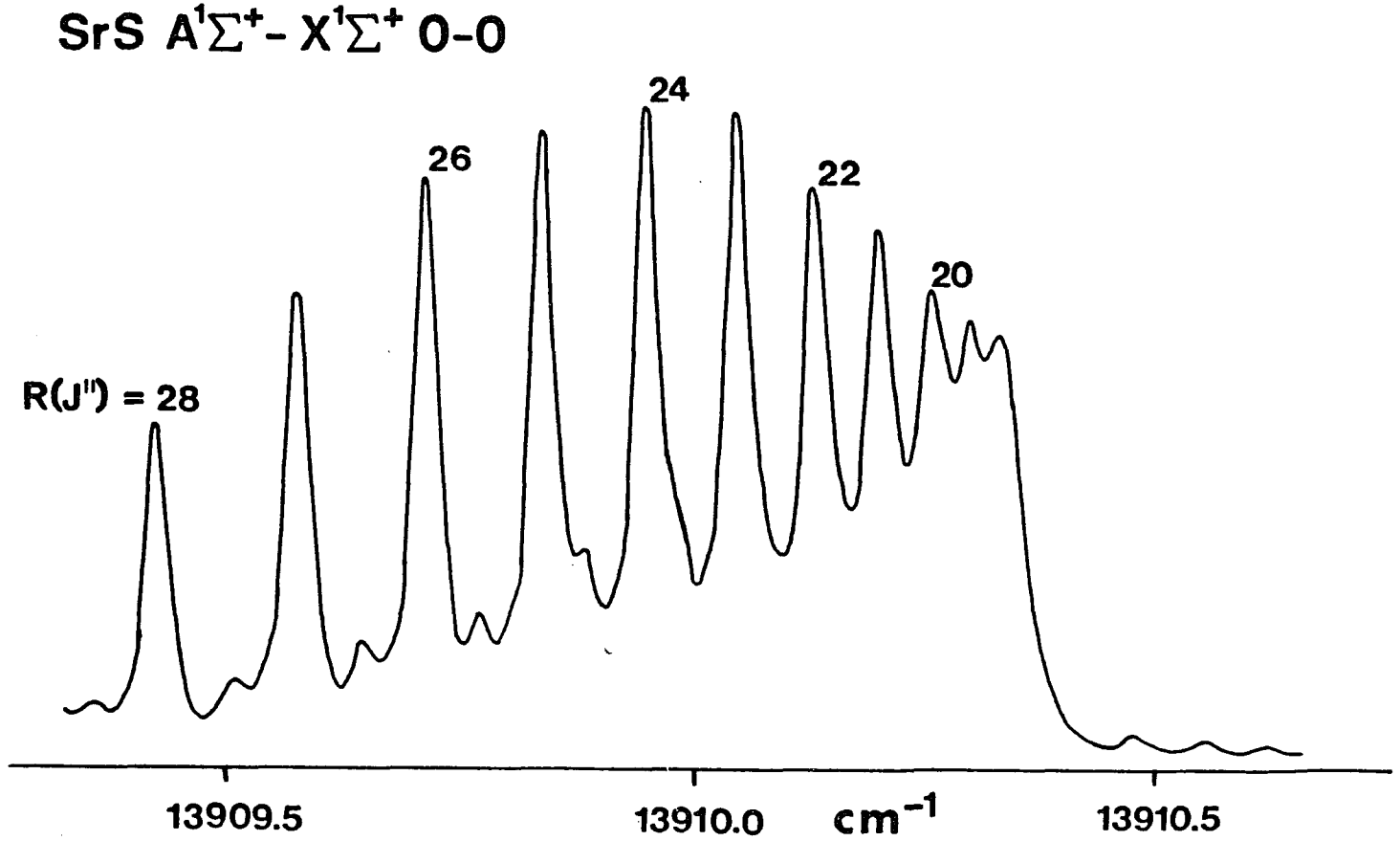
SrS $A^1\Sigma^+ - X^1\Sigma^+$ 0-0
R(J") = 28
26
24
22
20
13909.5
13910.0
cm^{-1}
13910.5

J = 24 appears strongest in this spectrum due to the placement of the monochromator at the 0-1 bandhead. Low J lines can be seen as the small features going into the bandhead.

Perturbations were observed in most of the vibrational levels in the excited state. The local perturbations observed are presented in Table II. The nature of the perturbing states are not known, since both homogeneous ($\Delta\Lambda = 0$) and heterogeneous ($\Delta\Lambda = \pm 1$) interactions fit the perturbations equally well. In all cases, the perturbations appeared to be sharp, indicating that the perturbing states have rotational constants quite different from that of the perturbed $A^1\Sigma^+$ excited state.

A perturbation in the P-branch of the 5-1 band is shown in Figure VI. The perturbed P(32) line is shifted a small amount lower in frequency from its expected position, while the perturbing line is shifted an equivalent amount in higher frequency. A similar pattern was observed in the 5-1 R-branch and in the 5-2 P- and R-branches. The behavior in the four branches is due to a perturbation at J = 31 in the v = 5 level of the $A^1\Sigma^+$ state.

The rotational lines from the nine bands (Appendix A) were simultaneously fit to the customary $^1\Sigma^+$ energy level expression.

$$E = T_v + BJ(J+1) - D[J(J+1)]^2 + H[J(J+1)]^3$$

The molecular constants resulting from the fit for vibrational levels in both the ground and excited states are presented in Table III. The ground state constants agree reasonably well but are more accurate than those from the work of Marcano and Barrow (11). The excited state

Table II. Observed Perturbations in $A^1\Sigma^+$ SrS.

v	J
0	40
1	0
3	43
3	59
5	31
5	45

Figure VI. Perturbation of the SrS $A^1\Sigma^+$ - $X^1\Sigma^+$ Spectrum.

The perturbation shown here is in the P-branch of the 5-1 band. The perturbation occurred at the rotational level J = 31 of the vibrational level v = 5 in the $A^1\Sigma^+$ state. The perturbed P(32) line is shifted by a small amount (around 0.1 cm^{-1}) lower in energy from its expected position as a result of the perturbation. The perturbing line, marked by the asterisk, is shifted an equivalent amount to higher energy.

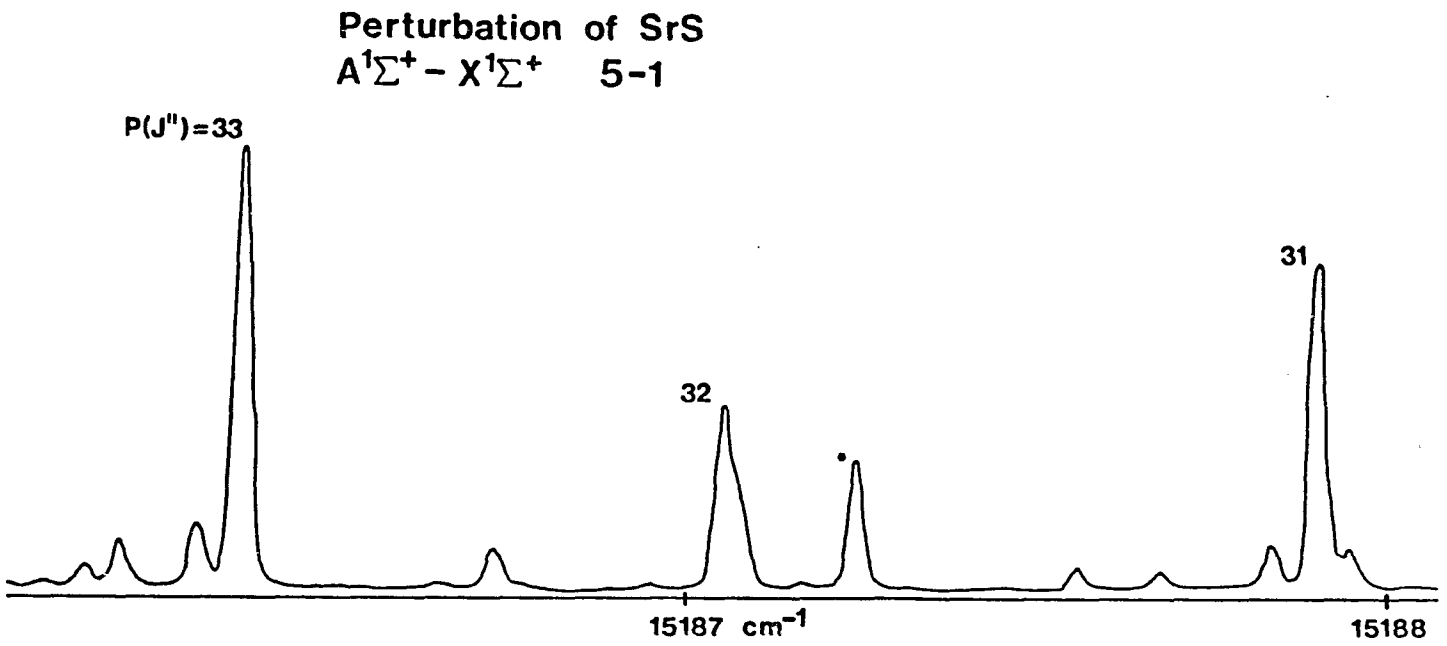
Perturbation of SrS
$A^1\Sigma^+ - X^1\Sigma^+$ 5-1
P(J")=33
32
31
15187 cm^{-1}
15188

Table III. Molecular Constants for $A^1\Sigma^+$ - $X^1\Sigma^+$ Transition of SrS (in cm^{-1}).

Level	T_v	B_v	$D_v \times 10^8$	$H_v \times 10^{10}$
		$X^1\Sigma^+$		
v = 0	0.0	0.1205652(29)[a]	4.894(64)	-
v = 1	385.70299(55)	0.1200876(29)	4.919(58)	-
v = 2	768.84690(69)	0.1196035(35)	4.86(13)	-
		$A^1\Sigma^+$		
v = 0	13908.3283(3)	0.1137945(30)	5.355(60)	-
v = 1	14246.3691(8)	0.1134215(31)	4.779(74)	-
v = 2	14583.3051(8)	0.1130825(33)	6.29(11)	-
v = 3	14919.3935(4)	0.1126042(34)	1.81(14)	-
v = 4	15254.0297(8)	0.1122499(55)	2.44(75)	-0.440(32)
v = 5	15589.2504(14)	0.1109100(65)	-44.38(60)	-0.948(17)

[a] The number in parenthesis represents one standard deviation uncertainty.

centrifugal distortion constants and the rotational constant H_v (especially for v = 3, 4, and 5) are not actual molecular rotational constants but only effective constants which resulted from the severe perturbations observed in these levels.

Lines from the 0-0, 0-1, 1-1, 2-1 bands and ground state combination differences between the 3-0 and 3-2 bands and between the 5-1 and 5-2 bands were also fit to a Dunham-type energy level expression (30) to determine equilibrium molecular constants (Table IV).

$$E_{vJ} = \Sigma\, Y_{kl}(v+1/2)^k[J(J+1)]^l$$

Due to the perturbed nature of the upper vibrational levels in the excited state, the 4-1 band was not included and the 3-0, 3-2, 5-1 and 5-2 combination differences were used in the fit. The use of combination differences essentially resulted in the removal of the most perturbed vibrational levels (v = 3,5) of the excited state from the fit, and allowed the v = 2 level of the ground state to be included. Again, the higher order excited state constants (particularly the D's and the H) are not actual molecular constants, but only effective constants that resulted from the severe perturbations of the excited state.

A Rydberg-Klein-Rees (RKR) potential curve (31) was calculated for the $X^1\Sigma^+$ and $A^1\Sigma^+$ states of SrS. The RKR potential curve turning points for the two states are given in Table V, and the curves drawn from the turning points are shown in Figure VII.

The RKR turning points and the dissociation energy

Table IV. Equilibrium Molecular Constants for the $A^1\Sigma^+$ - $X^1\Sigma^+$ Transition of SrS (in cm^{-1}).

Constant[a]		$X^1\Sigma^+$	$A^1\Sigma^+$
Y_{00} (T_e)		0.0	13932.7068(10)[b]
Y_{10} (ω_e)		388.2643(11)	339.1454(20)
$-Y_{20}$ ($\omega_e x_e$)		1.28032(38)	0.55237(67)
Y_{01} (B_e)		0.1208034(33)	0.1139895(38)
$-Y_{11}$ (α_e)		0.0004746(70)	0.0004048(38)
Y_{21} (γ_e)	x 10^6	-2.07(28)	16.6(14)
$-Y_{02}$ (D_e)	x 10^8	4.870(63)	6.16(11)
$-Y_{12}$ (β_e)	x 10^8	---	-2.56(16)
$-Y_{22}$	x 10^8	---	1.024(61)
Y_{03} (H_e)	x 10^{13}	---	-2.71(58)
r_e (Å)		2.439687(14)	2.511601(17)

[a] As defined in Ref. 34, pg. 92, 107 and 108.
[b] The number in parenthesis represents one standard deviation uncertainty.

Table Va. RKR Turning Points for SrS $X^1\Sigma^+$.

v	E_v (cm^{-1})	R_{min} (Å)	R_{max} (Å)
0.0	193.7831	2.38111	2.50299
0.5	386.9550	2.35812	2.53073
1.0	579.4867	2.34096	2.55266
1.5	771.3783	2.32682	2.57160
2.0	962.6298	2.31459	2.58865
2.5[a]	1153.2410	2.30373	2.60436
3.0	1343.2121	2.29389	2.61907
3.5	1532.5431	2.28487	2.63299
4.0	1721.2339	2.27651	2.64627
4.5	1909.2845	2.26871	2.65902
5.0	2096.6950	2.26138	2.67132

[a] Levels with v > 2 are extrapolations.

Table Vb. RKR Turning Points for SrS $A^1\Sigma^+$.

v	E_v (cm^{-1})	R_{min} (Å)	R_{max} (Å)
0.0	169.5137	2.44868	2.57903
0.5	338.6722	2.42389	2.60834
1.0	507.5544	2.40531	2.63136
1.5	676.1605	2.38991	2.65110
2.0	844.4903	2.37652	2.66874
2.5[a]	1012.5440	2.36455	2.68488
3.0	1180.3215	2.35363	2.69986
3.5	1347.8228	2.34354	2.71393
4.0	1515.0479	2.33412	2.72724
4.5	1681.9969	2.32524	2.73991
5.0	1848.6696	2.31682	2.75203

[a] Levels with v > 2 are extrapolations.

Figure VII. SrS $A^1\Sigma^+$ and $X^1\Sigma^+$ Potential Curves from the RKR Turning Points of Tabel V.

The $A^1\Sigma^+$ potential curve is shifted vertically downwards so that it has the same energy origin as the $X^1\Sigma^+$ curve. The $A^1\Sigma^+$ state is actually 13908.3283 cm^{-1} (T_{00}) above the $X^1\Sigma^+$ state.

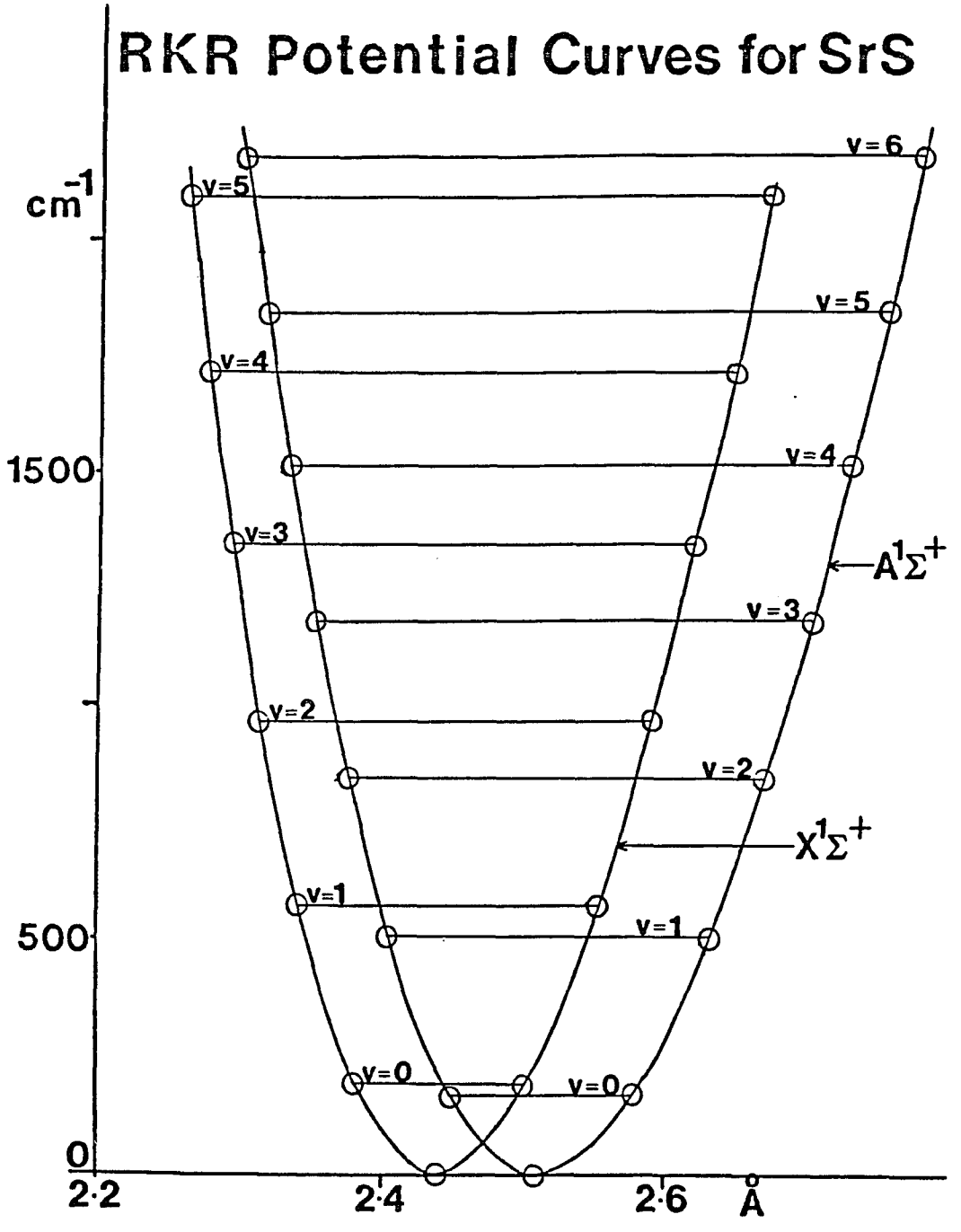
RKR Potential Curves for SrS
cm⁻¹
1500
500
0
2·2
2·4
2·6
Å
v=6
v=5
v=5
v=4
v=4
v=3
v=3
v=2
v=2
v=1
v=1
v=0
v=0
A¹Σ⁺
X¹Σ⁺

(D^0 = 3.48 eV, 32) of SrS were input to Hutson's centrifugal distortion program (33) to obtain predicted values for the rotational constants. Values obtained from Hutson's program for constants in the ground and excited states are presented in Table VI. The predicted centrifugal distortion constants of Table VI are closer to the "true values" than the corresponding constants determined by the fits presented in Table III, which were distorted by the $A^1\Sigma^+$ state perturbations. Finally, Franck-Condon intensity factors for transitions between the vibrational levels of the $A^1\Sigma^+$ state and the vibrational levels of the $X^1\Sigma^+$ state were calculated, and they are presented in Table VII.

Transitions involving the ^{86}Sr and ^{87}Sr isotopes of SrS were also observed in natural abundance (9.86%, 7.00%). The positions of the isotopic transitions were accurately predicted from the constants of Table IV, thus isotopic relationships appear to be well-behaved in SrS. Only a few of the isotopic lines were measured and they were not included in the fits.

Table VIa. Rotational Constants for Srs $X^1\Sigma^+$

Calculated from the Potential Curve of Table Va (in cm^{-1}).

Vibrational Level	B_v	$D_v \times 10^8$	$H_v \times 10^{15}$	$L_v \times 10^{20}$
		$X^1\Sigma^+$		
0	0.1205653	4.688	-2.192	-1.202
1	0.1200864	4.709	-2.769	-1.123
2	0.1196035	4.730	-3.455	-1.116
3[a]	0.1191163	4.749	-4.020	-0.895
4	0.1186252	4.768	-4.889	-0.931
5	0.1181297	4.786	-5.469	-0.825

[a] Values of vibrational levels with $v > 2$ are extrapolations.

Table VIb. Rotational Constants for SrS $A^1\Sigma^+$

Calculated from the Potential Curve of Table Vb (in cm^{-1}).

Vibrational Level	B_v	$D_v \times 10^8$	$H_v \times 10^{15}$	$L_v \times 10^{20}$
		$A^1\Sigma^+$		
0	0.1137949	5.139	8.865	0.075
1	0.1134245	5.120	15.056	-1.839
2	0.1130857	5.112	22.376	-4.263
3[a]	0.1127812	5.119	29.065	-6.035
4	0.1125090	5.136	36.770	-8.631
5	0.1122699	5.164	43.713	-9.035

[a] Values of vibrational levels with $v > 2$ are extrapolations.

Table VII. Franck-Condon Intensity Factors for SrS $A^1\Sigma^+ - X^1\Sigma^+$.

v' \ v"	0	1	2	3[a]	4	5
0	.5244	.3451	.1075	.0203	.0025	.0002
1	.3335	.0679	.3260	.2040	.0579	.0095
2	.1117	.3000	.2180	.2061	.2533	.1026
3[a]	.0255	.2001	.1771	.0552	.0968	.2578
4	.0043	.0688	.2327	.0745	.1134	.0300
5	.0005	.0154	.1150	.2198	.0181	.1432

[a] Values with v > 2 are extrapolations

Semi-Empirical Calculations on SrS

The Fenske-Hall computational method (35), a semi-empirical method of electronic structure calculation, was used to investigate the bonding of the SrS molecule. A brief description of the main features of the Fenske-Hall method and the SrS results are presented here.

The Fenske-Hall method applies various approximations (35) to the matrix elements of the Fock operator. The adjustable or empirical parameters used in extended Hückel calculations are not employed and the final parameters depend only on the choice of basis functions and internuclear distances.

For SrS, a molecular charge of zero and a bond length of 2.4397 Å were used in the calculation. The calculation predicts, as expected, that the ground state bonding in the molecule is predominately ionic. Treating the molecule as two closed shell atoms (strontium with an ionic charge of +2 and sulfur with an ionic charge of -2) results in a $^1\Sigma^+$ molecular ground state.

The calculation also predicts that the highest occupied molecular orbital is predominately sulfur $3p_z$ in character, and the lowest unoccupied molecular orbital is predominately strontium 5s in character. The transition to the LUMO from the HOMO is therefore a charge transfer from sulfur $3p_z$ to strontium 5s and results in an excited state having a +1 ionic charge on strontium and a -1 ionic

charge on sulfur. The differences in the ionic nature of the ground and excited states of SrS imply that the bond lengths for the states will be different, as was observed experimentally.

The electronic charge transfer of the excitation results in a σ hole in the sulfur $3p_z$-like σ molecular orbital and gives rise to two electronic excited states: $^1\Sigma^+$ and $^3\Sigma^+$. The $^1\Sigma^+$ state is the state observed in the present work.

Immediately below the HOMO are two occupied π orbitals which are predominately sulfur $3p_x$ and $3p_y$ in character. A charge transfer transition to the LUMO from either of these π orbitals results in a configuration that gives rise to $^1\Pi$ and $^3\Pi$ electronic excited states. These two states and the $^3\Sigma^+$ state have not been identified but may have been observed through perturbations of the $A^1\Sigma^+$ state.

The energies and configurations of the known SrS electronic states are shown in Figure VIII. The $A^1\Sigma^+ - X^1\Sigma^+$ was observed in the present work (13), and the $B^1\Sigma^+ - X^1\Sigma^+$ was observed by Marcano and Barrow (11). The energies of the $A'^1\Pi$ and $a^3\Pi$ states were calculated by Partridge, Langhoff and Bauschlicher (12) using ab initio methods. Finally, the $b^3\Sigma^+$ state probably lies between the $A'^1\Pi$ state and the $A^1\Sigma^+$ state.

Figure VIII. SrS Energy Level Diagram.

The energies and configurations of the lowest electronic states of SrS are shown. Arrow a) is the transition observed in the present work. Arrow b) is the transition observed by Marcano and Barrow (11). The energies of $A^1\Pi$ and the $a^3\Pi$ states were determined by Partridge, Langhoff and Bauschlicher (12) using ab initio methods. There is also a low-lying $b^3\Sigma^+$ state, probably between the $A'^1\Pi$ and $A^1\Sigma^+$ states.

SrS Energy Level Diagram

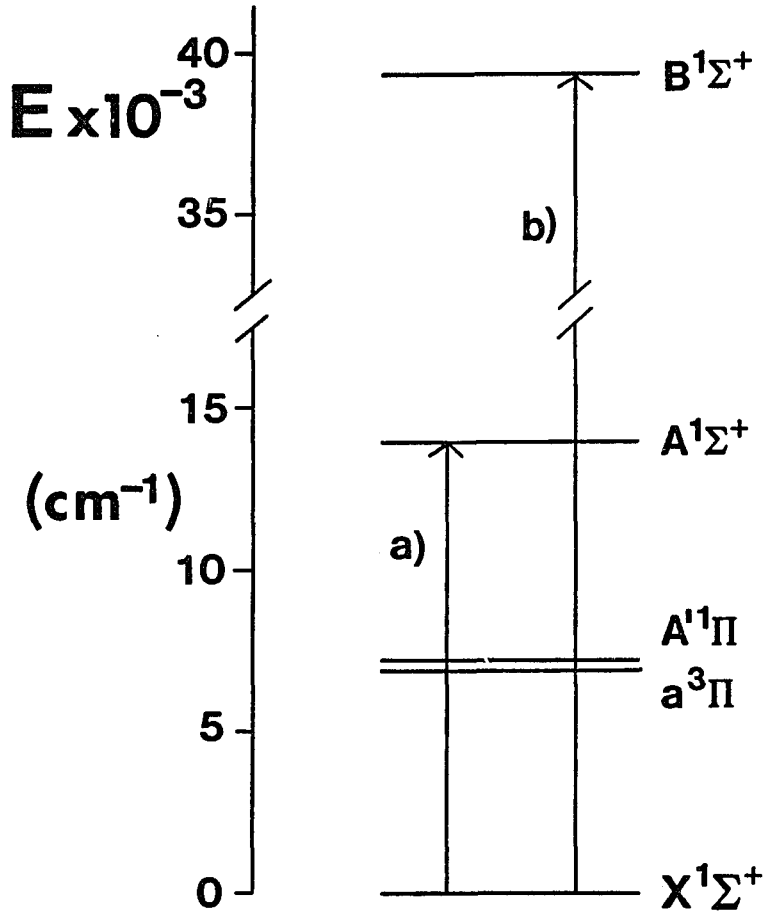

Valence Configurations

$\sigma^2 \pi^4 \sigma^2 \longrightarrow X^1\Sigma^+$

$\sigma^2 \pi^4 \sigma^1 \sigma^1 \longrightarrow A^1\Sigma^+$

$\sigma^2 \pi^3 \sigma^2 \sigma^1 \longrightarrow A'^1\Pi, a^3\Pi$

CHAPTER IV

ALKALINE EARTH BOROHYDRIDES

The tetrahydroborate ion (BH_4^-) forms a large number of interesting ionic and covalent complexes with metals (36,37). The coordination between the metal and the BH_4^- ion invariably occurs through bridging hydrogens, and interconversion between the various coordination modes is known in the liquid phase (36,37).

The BH_4^- is a very commonly used reducing agent. Nevertheless, very little is known about the spectroscopic properties of the metal-BH_4 complexes, particularly in the gas phase. Of the alkaline earth borohydrides, only $Be(BH_4)_2$ has been analyzed in the gas phase. Almenningen, Gundersen and Haaland (38,39) determined the $Be(BH_4)_2$ structure using electron diffraction methods.

Presented here is a low resolution laser analysis of gas phase calcium and strontium borohydride ($CaBH_4$ and $SrBH_4$) radicals (40). Also, lithium borohydride ($LiBH_4$) *ab initio* results (41-43) are briefly described.

Ab Initio Calculations on Lithium Borohydride

Lithium borohydride ($LiBH_4$) is similar to the calcium and strontium borohydride radicals. The extra nonbonding valence electron in the alkaline earth radicals is not expected to change their electronic structure by a large amount. While the structure of $LiBH_4$ has not been experimentally determined, three structures (Figure IX) seem most likely (41). Configuration a) is best described as a Li^+ ion coordinated to the face of the BH_4^- tetrahedron. Bonding is tridentate, or occurs between the Li^+ ion and three bridging hydrogens. Configuration b) is bidentate with respect to bridging hydrogens, and the Li^+ ion is on an edge of the BH_4^- tetrahedron. Finally, configuration c), with Li^+ coordinated to a BH_4^- vertex, is monodentate. The symmetry of the three configurations are C_{3v}, C_{2v}, and C_{3v} for the tri-, bi-, and monodentate structures, respectively.

The equilibrium geometry and potential energy surfaces of the three structures have been calculated by several authors (41-53) using ab initio methods. The ab initio calculations consistently indicate that the tridentate configuration, a), is the most stable. For the bidentate, b), structure, the total electronic energy is usually determined to be slightly higher, about 2-12 kcal/mole, depending on the basis sets used. The monodentate, c), configuration is much higher in energy, at about 20-35 kcal/mol higher than the tridentate structure.

Figure IX. Possible structures of Li^+-BH_4^- (Boldyrev et al., 41).

Three possible structures of $LiBH_4$ with Li^+ bonded to a BH_4^- core: a) tridentate (three bridging hydrogens), b) bidentate (two bridging hydrogens), and c) monodentate (one bridging hydrogen). Ab initio calculations (41-53) predict that the tridentate structure, a), is the most stable.

$LiBH_4$ Configurations

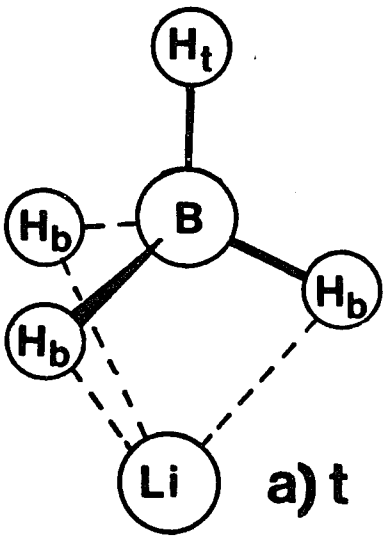

a) t

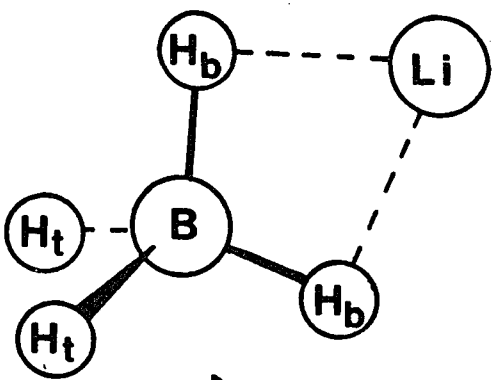

b) b

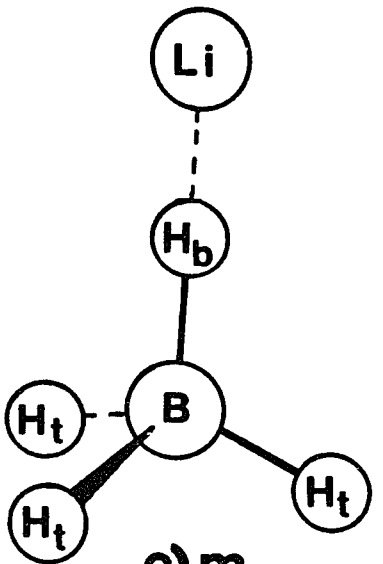

c) m

Since the barrier between the four possible tridentate configurations of $LiBH_4$ is low, fluxional behavior is expected (41-53). The suggested path for the fluxional bahavior is a) - b) - a)', where b), the bidentate configuration, is the saddle point of the transformation (Figure IX).

Baranov and Boldyrev (50) presented a nonrigid model for analysis of the fluxional behavior. In brief, four equivalent configurations with a Li cation situated over the centers of the four faces of a slightly distorted BH_4^- tetrahedron correspond to the four absolute minima on the energy surface. The external Li cation can move around the rigid tetrahedral BH_4^- core.

Using the model, Baranov and Boldyrev (50) numerically calculated the levels of large-amplitude migration motion of the cation. The lowest levels lying below the saddle points can be regarded as highly anharmonic bending vibrations, with an approximate frequency of 220 cm^{-1}. The levels above the barrier are very chaotic and can be considered as hindered rotations of the BH_4 group. Tunneling was shown to split each rotational energy level into a doublet of T and A_1 symmetry.

The metal-BH_4 stretching modes of $CaBH_4$ and $SrBH_4$ were analyzed in the present experiment. If tunneling occurred, it would be characterized by doubling in the rotational lines. A laser analysis at high resolution could possibly resolve the rotational doubling, but no doubling has been observed yet.

Experimental Details

The calcium and strontium borohydrides were produced in a Broida oven (1) by the reaction of Ca or Sr with diborane (B_2H_6). The Ca or Sr metal was vaporized from a resistively heated crucible, carried to the reaction region by argon, and reacted with the oxidant, diborane. The diborane was stored as a solid in a liquid nitrogen bath. During the experiment, the diborane was melted with a pentane/liquid N_2 bath (-130°C) and added as a gas to the Broida oven. The pressures were approximately 1 Torr argon and 0.035 Torr diborane.

The diborane was prepared by slowly adding sodium borohydride ($NaBH_4$) to heated polyphosphoric acid under vacuum. The diborane gas produced was collected with a liquid N_2 bath.

Two types of low resolution spectra were recorded. Laser excitation spectra were obtained by scanning a broadband (1 cm^{-1}) CW dye laser through a spectral region where $CaBH_4$ or $SrBH_4$ absorb and detecting total fluorescence through red pass filters with a photomultiplier tube. Resolved fluorescence spectra were obtained by fixing the dye laser at the frequency of a $CaBH_4$ or $SrBH_4$ molecular transition and scanning the wavelength of a 0.32 m monochromator to detect laser induced fluorescence.

In similar Broida oven experiments (3-5), a second dye laser tuned to the Ca or Sr atomic line was required to promote the reaction

between the alkaline earth vapor and the various oxidants. The reaction between Ca or Sr with diborane, however, was vigorous enough to be detected without the use of the second dye laser to excite the metal.

Results and Discussion

The spectra of the calcium and strontium borohydrides were assigned by comparison to the spectra of other alkaline earth molecules (3-5). Two transitions to excited states were observed, and these were assigned $\tilde{A}^2A_1$ - $\tilde{X}^2A_1$, $\tilde{B}^2E_{1/2}$ - $\tilde{X}^2A_1$, and $\tilde{B}^2E_{3/2}$ - $\tilde{X}^2A_1$. The presence of a spin-orbit splitting (and its magnitude) in the ^2E transition strongly suggest a symmetric top structure. The structural assignment of C_{3v} symmetry is consistent with the predicted lowest energy structure, a), of the ab initio calculations discussed previously.

Figure X is a portion of a $CaBH_4$ laser excitation scan. The 0-0 bands of the $\tilde{A}^2A_1$ - $\tilde{X}^2A_1$ and the $\tilde{B}^2E$ - $\tilde{X}^2A_1$ transitions are labeled. The 1-0 and 2-0 bands of the $\tilde{A}^2A_1$ - $\tilde{X}^2A_1$ transition appear as the small features at approximately 6550 Å and 6350 Å respectively. The 1-0 and 0-1 bands of the $\tilde{B}^2E$ - $\tilde{X}^2A_1$ transition appear at approximately 6290 Å and 6675 Å respectively. The 3/2 spin component of the $\tilde{B}^2E$ state at higher energy is slightly more intense than the 1/2 spin component, and the spin-orbit coupling constant of the $\tilde{B}^2E$ state is approximately 65 cm^{-1} for $CaBH_4$ and 202 cm^{-1} for $SrBH_4$. These values are somewhat lower than what is typically observed for calcium (65-75 cm^{-1}) and strontium (260-290 cm^{-1}) with other ligands (3-5). The low values are attributed to the high number of bridging hydrogens involved in the metal-ligand bond that act to diminish the spin-orbit interaction.

Figure X. Laser Excitation Spectrum of $CaBH_4$.

The 0-0 vibrational bands of the $\tilde{B}^2E$ - $\tilde{X}^2A_1$ and $\tilde{A}^2A_1$ - $\tilde{X}^2A_1$ transitions are labeled. Only the Ca-BH_4 stretching modes have Franck-Condon activity. The relative intensities of the two transitions are distorted by the effects of variation in laser power with frequency and the use of a red-pass filter. The small features at 6550 Å and 6350 Å are the 1-0 and 2-0 bands of the $\tilde{A}^2A_1$ - $\tilde{X}^2A_1$ transition, and the small features at 6290 Å and 6675 Å are the 1-0 and 0-1 bands of the $\tilde{B}^2E$ - $\tilde{X}^2A_1$ transition.

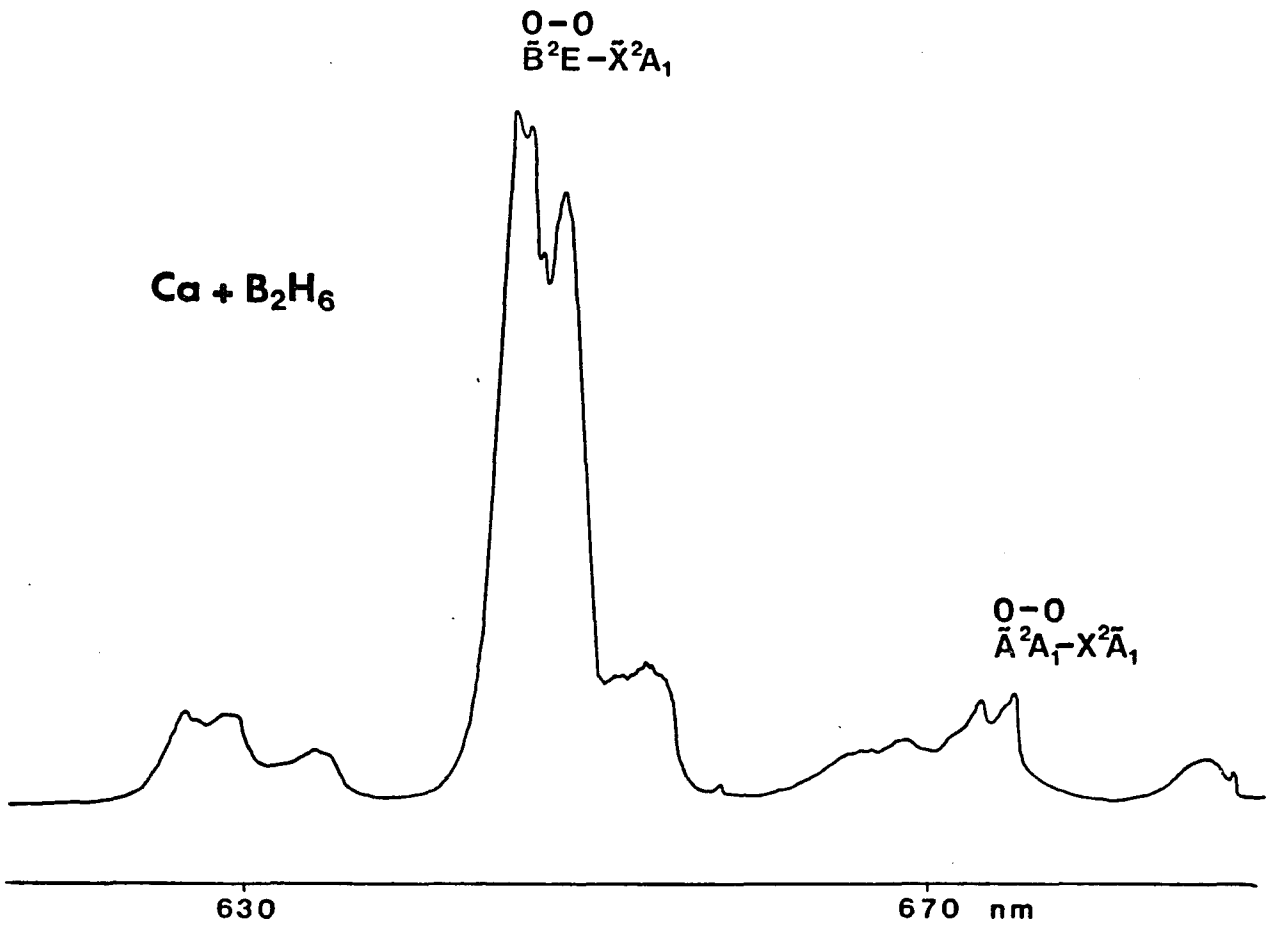
0-0
$\tilde{B}^2E-\tilde{X}^2A_1$
$Ca + B_2H_6$
0-0
$\tilde{A}^2A_1-X^2\tilde{A}_1$
630
670 nm

The laser excitation spectrum of $SrBH_4$ is shown in Figure XI. The 0-0 bands of the $\tilde{B}^2E$ - $\tilde{X}^2A_1$ transitions and the $\tilde{A}^2A_1$ - $\tilde{X}^2A_1$ transition are labeled. The large unlabeled peak is a blend of the $\tilde{B}^2E$ - $\tilde{X}^2A_1$ 0-1 band and the $\tilde{A}^2A_1$ - $\tilde{X}^2A_1$ 1-0 band. The asterisk marks the Sr atomic line at 6892 Å.

A portion of a $CaBH_4$ resolved fluorescence spectrum is shown in Figure XII. To record this spectrum, the dye laser was fixed at the frequency of the 1/2 spin component of the $\tilde{B}^2E$ state while the monochromator was scanned. By coincidence, the laser is also positioned at the frequency of the 1-0 band of the $\tilde{A}^2A_1$ - $\tilde{X}^2A_1$ transition. The asterisk marks the scattered light from the laser. The blue (higher energy) side of the first expanded feature at approximately 6550 Å consists mostly of fluorescence to the vibrational level v = 1 of the $\tilde{X}^2A_1$ state from the v = 0 level of the $\tilde{B}^2E_{1/2}$ state. The red (lower energy) side of the feature is mostly due to fluorescence from the v = 0 level of the $\tilde{A}^2A_1$ state to the v = 0 level $\tilde{X}^2A_1$ state. The other two expanded features at approximately 6900 Å and 7300 Å also result from mixtures of emission to excited vibrational levels of the ground $\tilde{X}^2A_1$ state from the v = 0 level of the $\tilde{B}^2E$ state and the v = 0 level of the $\tilde{A}^2A_1$ state.

Band origins determined for $CaBH_4$ and $SrBH_4$ are presented in Table VIII. For each band, the origin was determined by averaging values from both laser excitation and resolved fluorescence scans. Finally, vibrational frequencies for the three observed states were determined from the band origins and are presented in Table IX.

Figure XI. Laser Excitation Spectrum of $SrBH_4$.

The 0-0 vibrational bands of the $\tilde{B}^2E$ - $\tilde{X}^2A_1$ and $\tilde{A}^2A_1$ - $\tilde{X}^2A_1$ transitions are labeled. Like $CaBH_4$, only the Sr-BH_4 stretching modes display Franck-Condon activity. The feature at 7075 Å is a blend of the 1-0 band of the $\tilde{A}^2A_1$ - $\tilde{X}^2A_1$ transition and the 0-1 vibration of the $\tilde{B}^2E$ - $\tilde{X}^2A_1$ transition. The asterisk marks the Sr $^3P_1$ - $^1S_0$ atomic line.

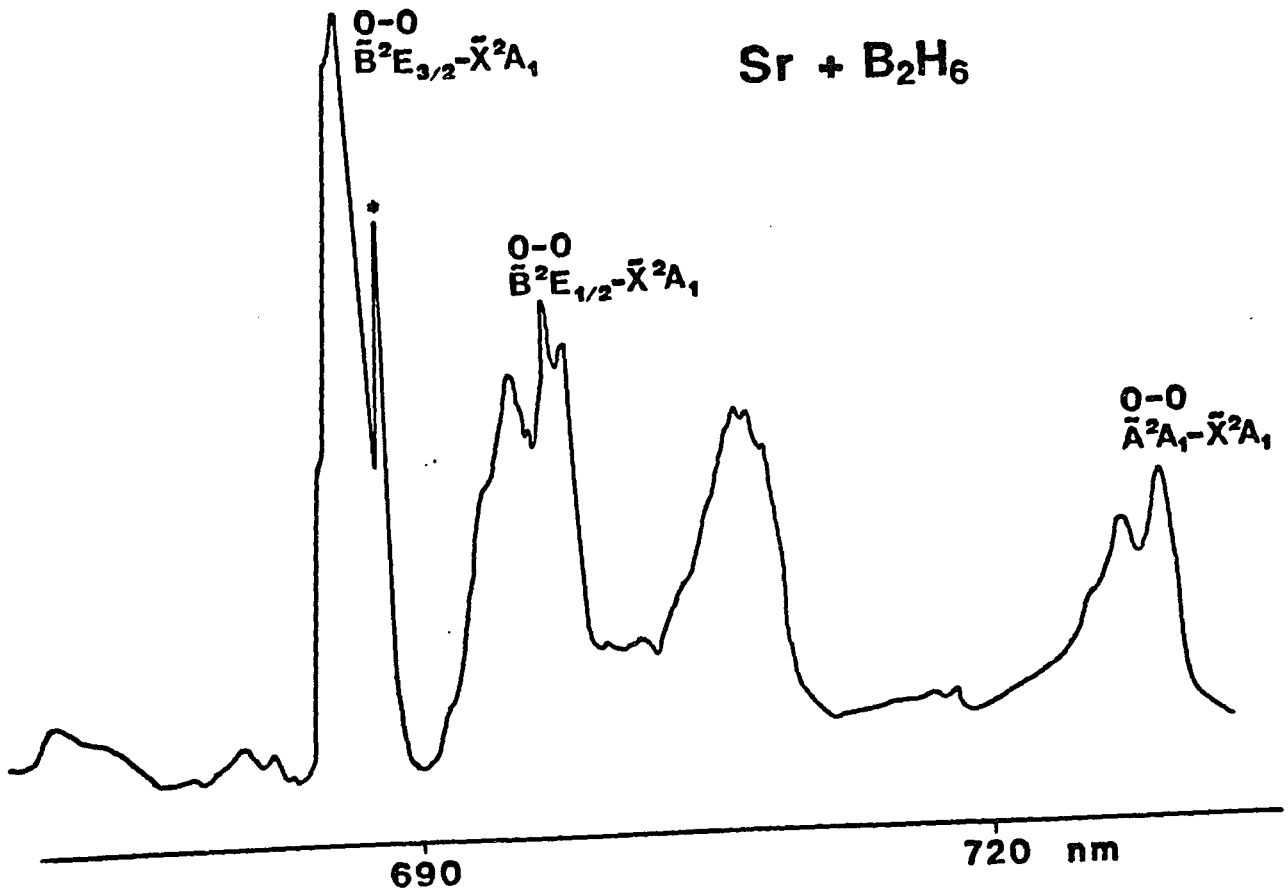
0-0
$\tilde{B}^2E_{3/2}$-$\tilde{X}^2A_1$
Sr + B_2H_6
0-0
$\tilde{B}^2E_{1/2}$-$\tilde{X}^2A_1$
0-0
$\tilde{A}^2A_1$-$\tilde{X}^2A_1$
690
720 nm

Figure XII. Resolved Fluorescence Spectrum of $CaBH_4$.

The frequency of the dye laser was held fixed on the 1/2-spin component of the 0-0 band $\tilde{B}^2E$ - $\tilde{X}^2A_1$ transition. The laser scatter is marked by the asterisk. By coincidence, the laser is also exciting the 1-0 vibration of the $\tilde{A}^2A_1$ - $\tilde{X}^2A_1$ transition. The features at higher wavelength (the three expanded peaks) result from a mixture of emission to excited vibrational levels of the ground $\tilde{X}^2A_1$ state from the v = 0 level of the $\tilde{B}^2E$ state and from vibrational levels of the $\tilde{A}^2A_1$ state.

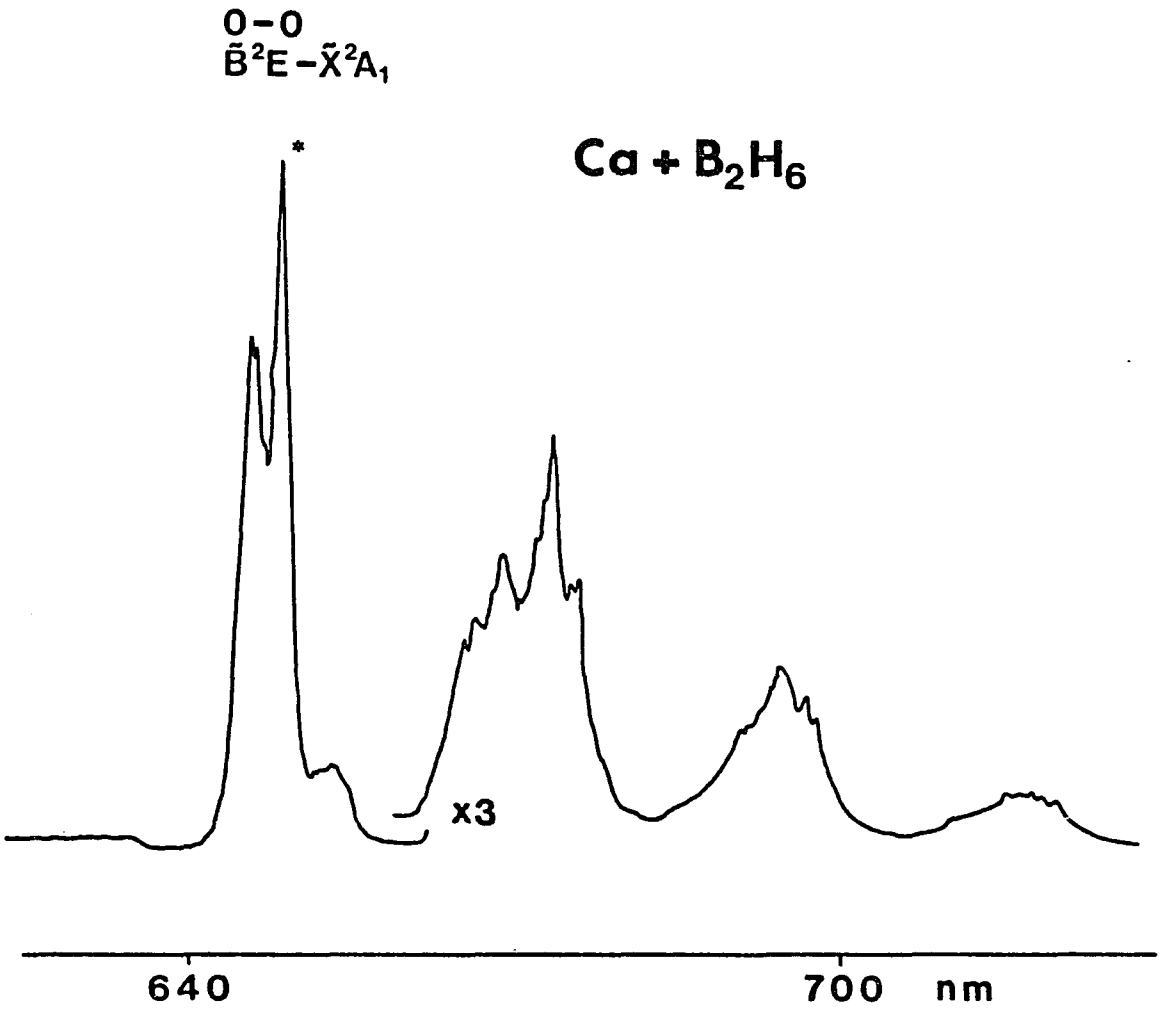
0-0
$\tilde{B}^2E-\tilde{X}^2A_1$
*
Ca + B_2H_6
x3
640
700 nm

Table VIII. Band Origins of $CaBH_4$ and $SrBH_4$ Vibronic Transitions (in cm^{-1}).

Band	$CaBH_4$	$SrBH_4$
	$\tilde{B}^2E_{3/2} - \tilde{X}^2A_1$	
2-0	-	15347[a]
1-0	15933	14940
0-0	15466	14518
0-1	-	14112
	$\tilde{B}^2E_{1/2} - \tilde{X}^2A_1$	
2-0	-	15144
1-0	15866	14735
0-0	15401	14316
0-1	14948	13915
	$\tilde{A}^2A_1 - \tilde{X}^2A_1$	
2-0	15740	-
1-0	15272	14090
0-0	14799	13669
0-1	14341	13274
0-2	13889	-
0-3	13424	-

[a] Errors are approximately ± 10 cm^{-1}.

Table IX. Vibrational Frequencies for $CaBH_4$ and $SrBH_4$ (in cm^{-1}).

State	$CaBH_4$	$SrBH_4$
$\tilde{B}^2E$	465[a]	421
$\tilde{A}^2A_1$	473	420
$\tilde{X}^2A_1$	457	399

[a] Errors are approximately ± 10 cm^{-1}.

The excited state ordering of the alkaline earth borohydrides is surprising. Previously analyzed symmetric top molecules (3,4) ($CaCH_3$, $SrCH_3$ and $SrOCH_3$) have ^2E states lower in energy than $^2A_1$ states, whereas in the borohydrides, the ordering is reversed.

The borohydride spectra were also compared to calcium and strontium formate (CaO_2CH and SrO_2CH) spectra (5). Attempts to assign the formate spectra were previously unsuccessful. As in the borohydride, the formate ^2E state appeared to be higher in energy than the $^2A_1$ state, and opposite the ordering in the methoxide and methyl derivatives. Due to their spectral similarities, however, the borohydride and formate excited state assignments appear to be correct.

The alkaline earth borohydride and formate molecules share one striking similarity. In each, bonding occurs off the metal-ligand axis with bridging ligand atoms (three hydrogens for the borohydrides and two oxygens for the formates). The bridging atoms have a partial negative charge. When they point towards the off-axis Ca^+ and Sr^+ p and d orbitals containing the excited electron, the π-like bonding orbitals are destablized relative to the on-axis σ-like orbitals.

In the cases of the methyl and methoxide derivatives, bonding occurs on the metal-ligand axis. The negative charge of the ligand points to the on-axis orbitals of the cation. When containing the excited extra electron, the resulting σ-like molecular orbitals are destablized.

Figure XIII is a correlation diagram of the energy levels resulting from ligand and alkaline earth cation interactions. The

Figure XIII. Correlation Diagram of Alkaline Earth Metal-Ligand Interactions.

The diagram shows the effects of various ligands perturbing the metal ion (Sr^+ and Ca^+) atomic orbitals. The ordering of the first excited states, ^2E and $^2A_1$, for MBH_4 radicals is reversed when compared with the MCH_3 radicals. The difference in ordering is attributed to differences in ionic bonding. For the MCH_3 molecules, bonding occurs on the metal-ligand axis, between the alkaline earth cation M^+ and the negatively charged carbon. For the MBH_4 molecules, however, bonding also occurs off the metal-ligand axis, between the cation M^+ and three bridging hydrogens which bear a partial negative charge. This partial negative charge destabilizes the off-axis ^2E state relative to the $^2A_1$ state. The atomic orbital character of ^2E and $^2A_1$ states and the nature of the metal-ligand bond determine the relative ordering of the states.

CORRELATION DIAGRAM

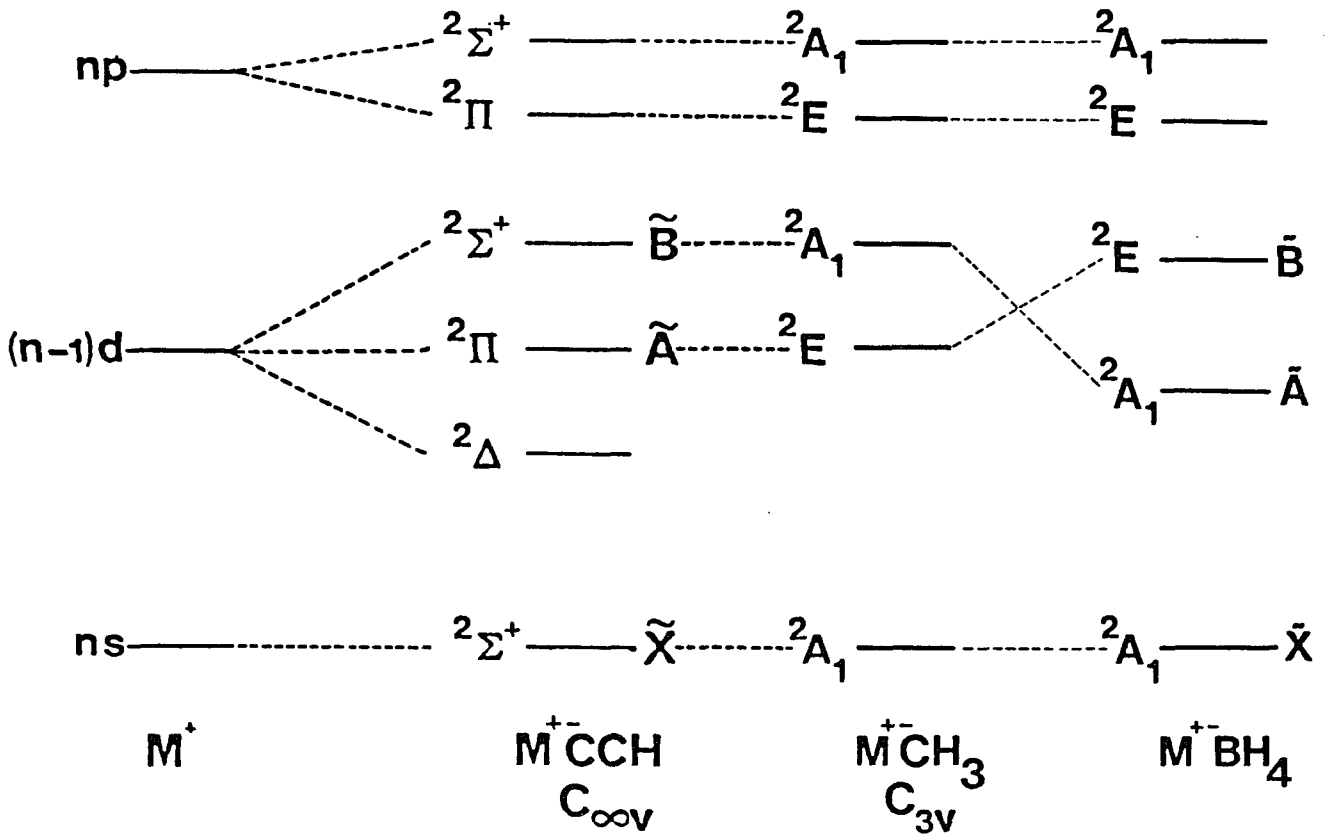

perturbing ligands reduce the symmetry of the metal atomic orbitals and remove some of their degeneracies. The diagram shows the $^2A_1$ and ^2E excited state ordering differences in MCH_3 and MBH_4.

Calcium borohydride is currently being analyzed (54) using high resolution laser techniques in an attempt to make a definite assignment of the states observed, and to determine the molecular rotational constants. Several bands of the $\tilde{B}^2E$ - $\tilde{X}^2A_1$ transition have been recorded and the resulting rotational transitions were fit to a $^2\Pi$ - $^2\Sigma^+$ Hamiltonian. To achieve a reasonable fit, large Λ-doubling interaction constants were required, implying highly perturbed states. The nature of the perturbations have not yet been established, and the project is still under investigation.

APPENDIX A

OBSERVED ROTATIONAL LINE POSITIONS FOR SrS $A^1\Sigma^+ - X^1\Sigma^+$

(IN CM^{-1})

Table Ia. Observed Line Positions for SrS $A^1\Sigma^+ - X^1\Sigma^+$ (in cm^{-1}).

0-0 Band				
J"	P(J")	$\Delta\nu$[a]	R(J")	$\Delta\nu$
0			13908.5562	.0003
1	13908.0868	-.0004	13908.7713	.0014
2	13907.8333	.0008	13908.9698	-.0006
3	13907.5648	.0005	13909.1599	.0025
4	13907.2832	.0007	13909.3334	.0026
5	13906.9878	.0005	13909.4918	.0011
6	13906.6742	-.0042	13909.6369	-.0001
7	13906.3547	-.0013	13909.7703	.0006
8	13906.0244	.0042	13909.8888	-.0001
9	13905.6691	-.0016	13909.9955	.0009
10	13905.3055	-.0023	13910.0889	.0022
11	13904.9324	.0011	13910.1656	.0004
12	13904.5427	.0014		
13	13904.1382	.0005		
14	13903.7215	.0009		
15	13903.2923	.0024		
16	13902.8477	.0019		
17	13902.3903	.0022		
18	13901.9189	.0021		
19	13901.4343	.0023		
20	13900.9344	.0007		
21	13900.4222	.0004		
22	13899.8987	.0022		
23	13899.3597	.0022	13910.0472	-.0014
24	13898.8040	-.0010	13909.9505	-.0001
25	13898.2359	-.0031	13909.8387	-.0002
26	13897.6585	-.0009	13909.7120	-.0017
27	13897.0655	-.0008	13909.5719	-.0029
28	13896.4594	-.0002	13909.4218	-.0005
29	13895.8377	-.0017	13909.2550	-.0012
30	13895.2034	-.0022	13909.0765	.0001
31	13894.5596	.0013	13908.8797	-.0033
32	13893.8952	-.0022	13908.6729	-.0031
33	13893.2201	-.0029	13908.4523	-.0030
34	13892.5304	-.0046	13908.2173	-.0037
35	13891.8311	-.0023	13907.9678	-.0053
36	13891.1139	-.0044	13907.7030	-.0084
37	13890.3847	-.0049	13907.4279	-.0082
38	13889.6404	-.0069	13907.1312	-.0160

[a] Observed-Calculated line positions using the constants of Table III.

Table Ia. The Observed Line Positions for SrS $A^1\Sigma^+ - X^1\Sigma^+$ (in cm^{-1}).

0-0 Band (cont.)

J"	P(J")	$\Delta\nu$[a]	R(J")	$\Delta\nu$
39	13888.8874	-.0041	13906.7231	-.1215
40	13888.1085	-.0135	13906.5442	.0159
41	13887.2176	-.1214	13906.2067	.0084
42	13886.5603	.0179	13905.8587	.0041
43	13885.7410	.0087	13905.5004	.0032
44	13884.9136	.0051	13905.1280	.0019
45	13884.0738	.0027	13904.7421	.0008
46	13883.2241	.0039	13904.3373	-.0055
47	13882.3575	.0019	13903.9266	-.0040
48	13881.4784	.0010	13903.5056	.0009
49	13880.5861	.0005	13903.0650	.0000
50	13879.6805	.0002	13902.6108	-.0007
51	13878.7607	-.0005	13902.1460	.0016
52	13877.8294	.0008	13901.6638	.0004
53	13876.8853	.0030	13901.1693	.0006
54	13875.9246	.0022	13900.6607	.0004
55	13874.9511	.0022	13900.1392	.0012
56	13873.9625	.0008	13899.6015	-.0005
57	13872.9614	.0005	13899.0528	.0006
58	13871.9458	-.0006	13898.4874	-.0012
59	13870.9198	.0015	13897.9118	.0007
60	13869.8779	.0014	13897.3212	.0013
61	13868.8214	.0003	13896.7147	-.0001
62	13867.7501	-.0018	13896.0983	.0024
63	13866.6687	-.0004	13895.4635	.0003
64	13865.5755	.0029	13894.8170	.0004
65	13864.4614	-.0010	13894.1528	-.0034
66	13863.3360	-.0026	13893.4821	.0002
67			13892.7948	.0011
68			13892.0904	-.0013
69			13891.3731	-.0026
70			13890.6454	-.0005

[a] Observed-Calculated line positions using the constants of Table III.

Table Ib. The Observed Line Positions for SrS $A^1\Sigma^+ - X^1\Sigma^+$ (in cm^{-1}).

0-1 Band				
J"	P(J")	$\Delta\nu$[a]	R(J")	$\Delta\nu$
4	13521.5876	-.0015		
5	13521.2991	.0005		
6	13520.9989	.0034		
7	13520.6803	.0005		
8	13520.3518	.0002		
9	13520.0099	-.0009		
10	13519.6581	.0008		
11	13519.2931	.0018		
12	13518.9120	-.0008		
13	13518.5222	.0006		
14	13518.1200	.0021		
15	13517.7013	-.0003		
16	13517.2715	-.0012		
17	13516.8326	.0014		
18	13516.3763	-.0009		
19	13515.9106	.0000		
20	13515.4307	-.0006		
21	13514.9455	.0059	13524.7183	-.0033
22	13514.4336	-.0016	13524.6683	-.0035
23	13513.9201	.0019	13524.6097	.0004
24	13513.3886	-.0001	13524.5346	.0004
25	13512.8471	.0005	13524.4444	-.0021
26	13512.2929	.0011	13524.3450	-.0010
27	13511.7234	-.0011	13524.2336	.0006
28	13511.1424	-.0022	13524.1069	-.0004
29	13510.5507	-.0014	13523.9695	.0006
30	13509.9461	-.0009	13523.8177	-.0001
31	13509.3291	-.0002	13523.6521	-.0019
32			13523.4748	-.0028
33	13508.0524	-.0038	13523.2864	-.0021
34	13507.3971	-.0036	13523.0826	-.0041
35	13506.7291	-.0035	13522.8680	-.0042
36	13506.0473	-.0046	13522.6436	-.0014
37	13505.3572	-.0014	13522.3989	-.0062
38	13504.6463	-.0063	13522.1373	-.0152
39	13503.9251	-.0090	13521.8408	-.0464
40	13503.1864	-.0166	13521.6298	.0206
41	13502.3337	-.1255	13521.3252	.0068
42	13501.7186	.0158	13521.0203	.0054

[a] Observed-Calculated line positions using the constants of Table III.

Table Ib. The Observed Line Positions for SrS $A^1\Sigma^+ - X^1\Sigma^+$ (in cm^{-1}).

0-1 Band (cont.)

J"	P(J")	$\Delta\nu$[a]	R(J")	$\Delta\nu$
43	13500.9425	.0088	13520.7011	.0024
44	13500.1594	.0073	13520.3718	.0021
45	13499.3631	.0053	13520.0310	.0030
46	13498.5501	-.0008	13519.6760	.0024
47	13497.7350	.0037	13519.3068	.0005
48	13496.9000	.0009		
49	13496.0549	.0007		
50	13495.1979	.0012		
51	13494.3271	.0006		
52	13493.4448	.0011		
53	13492.5469	-.0013		
54	13491.6387	-.0014		
55	13490.7191	-.0001		
56	13489.7871	.0014		
57	13488.8392	-.0003		
58	13487.8788	-.0018		
59	13486.9081	-.0010		
60	13485.9232	-.0016		
61	13484.9248	-.0030		
62	13483.9156	-.0026		
64	13481.8641	.0034		
65	13480.8154	.0025		
66	13479.7535	.0012		
67	13478.6777	-.0013		
68	13477.5926	-.0004		
69	13476.4929	-.0013		
70	13475.3828	.0001		

[a] Observed-Calculated line positions using the constants of Table III.

Table Ic. The Observed Line Positions for SrS $A^1\Sigma^+ - X^1\Sigma^+$ (in cm^{-1}).

1-1 Band

J"	P(J")	$\Delta\nu$[a]	R(J")	$\Delta\nu$
1			13861.2266	.1202
2			13861.3962	.0896
3	13860.0244	.1188	13861.5547	.0612
4	13859.7125	.0871	13861.7097	.0428
5	13859.3988	.0669	13861.8544	.0273
6	13859.0660	.0409	13861.9889	.0150
7			13862.1185	.0111
8			13862.2319	.0043
9	13858.0336	.0089	13862.3353	.0009
10	13857.6676	.0030	13862.4295	.0017
11	13857.2956	.0044	13862.5079	-.0000
12	13856.9052	.0008	13862.5740	-.0007
13	13856.5031	-.0012	13862.6247	-.0035
14	13856.0933	.0023	13862.6662	-.0020
15	13855.6649	.0006		
16	13855.2257	.0014		
17	13854.7705	-.0005		
18	13854.3031	-.0012		
19	13853.8285	.0041		
20	13853.3286	-.0026		
21	13852.8190	-.0057		
22	13852.3035	-.0013		
23	13851.7699	-.0018		
24	13851.2254	.0001		
25	13850.6637	-.0019		
26	13850.0859	-.0066		
27	13849.5066	.0004		
28	13848.9057	-.0010	13861.8226	-.0052
29	13848.2903	-.0035	13861.6674	-.0003
30	13847.6589	-.0087	13861.4958	.0016
31	13847.0300	.0018	13861.3075	.0002
32	13846.3754	-.0000	13861.1084	.0013
33	13845.7108	.0014	13860.8942	.0007
34	13845.0315	.0013	13860.6667	.0001
35	13844.3396	.0020	13860.4285	.0022
36	13843.6297	-.0021	13860.1747	.0020
37	13842.9111	-.0016	13859.9046	-.0011
38	13842.1838	.0035	13859.6265	.0011
39	13841.4370	.0023	13859.3321	.0004

[a] Observed-Calculated line positions using the constants of Table III.

Table Ic. The Observed Line Positions for SrS $A^1\Sigma^+ - X^1\Sigma^+$ (in cm^{-1}).

1-1 Band (cont.)

J"	P(J")	$\Delta\nu$[a]	R(J")	$\Delta\nu$
40	13840.6769	.0011	13859.0234	-.0013
41	13839.9048	.0011	13858.7098	.0055
42	13839.1139	-.0044	13858.3778	.0072
43	13838.3182	-.0014	13858.0257	.0022
44	13837.5069	-.0008	13857.6639	.0009
45	13836.6821	-.0004	13857.2894	.0002
46	13835.8420	-.0022	13856.9049	.0028
47	13834.9916	-.0009	13856.5028	.0012
48	13834.1260	-.0016	13856.0908	.0030
49	13833.2463	-.0032	13855.6592	-.0014
50	13832.3540	-.0041	13855.2207	.0007

[a] Observed-Calculated line positions using the constants of Table III.

Table Id. The Observed Line Positions for SrS $A^1\Sigma^+ - X^1\Sigma^+$ (in cm^{-1}).

2-1 Band

J"	P(J")	$\Delta\nu$[a]	R(J")	$\Delta\nu$
1	14197.3651	.0031	14198.0430	.0025
2	14197.1141	.0063	14198.2390	.0004
3	14196.8392	-.0004	14198.4240	.0013
4	14196.5588	.0014		
6	14195.9513	.0003		
7	14195.6259	-.0008		
8	14195.2874	-.0011		
9	14194.9347	-.0016		
10	14194.5708	.0008		
11	14194.1863	-.0034		
12	14193.7929	-.0026		
17	14191.6123	-.0014		
18	14191.1322	-.0031		
19	14190.6416	-.0012		
20	14190.1365	.0002		
21	14189.6197	.0040		
22	14189.0793	-.0018		
23	14188.5299	-.0025	14199.1515	-.0041
24	14187.9713	.0016	14199.0411	-.0032
25	14187.3942	.0014	14198.9163	-.0026
26	14186.8014	-.0005	14198.7778	-.0015
27	14186.1970	.0001	14198.6278	.0023
28	14185.5801	.0022	14198.4576	-.0000
29	14184.9503	.0056	14198.2743	-.0012
30	14184.2967	-.0007	14198.0783	-.0009
31	14183.6353	-.0007	14197.8672	-.0014
32	14182.9591	-.0013	14197.6472	.0033
33	14182.2726	.0018	14197.4068	.0019
34	14181.5685	.0016	14197.1503	-.0014
35	14180.8494	.0004	14196.8885	.0043
36			14196.6066	.0042
37	14179.3689	-.0016	14196.3072	.0008
38	14178.6108	.0008	14195.9955	-.0005
39	14177.8354	.0001	14195.6716	.0002
40	14177.0468	.0004	14195.3298	-.0026
41	14176.2452	.0019	14194.9791	.0001
42	14175.4279	.0020	14194.6080	-.0034

[a] Observed-Calculated line positions using the constants of Table III.

Table Ie. The Observed Line Positions for SrS $A^1\Sigma^+ - X^1\Sigma^+$ (in cm^{-1}).

3-0 Band

J"	P(J")	$\Delta\nu$[a]	R(J")	$\Delta\nu$
0			14919.6181	-.0006
1	14919.1547	.0023	14919.8320	.0040
2	14918.8977	.0023	14920.0187	-.0027
3	14918.6203	-.0021	14920.2001	.0013
4	14918.3322	-.0013	14920.3624	.0020
5	14918.0295	.0008	14920.5063	.0003
6	14917.7085	.0005	14920.6359	.0002
7	14917.3683	-.0031	14920.7521	.0026
8	14917.0142	-.0047	14920.8496	.0023
9	14916.6504	-.0001	14920.9292	-.0001
10	14916.2684	.0022	14920.9969	.0015
11	14915.8671	.0011		
12	14915.4507	.0007		
13	14915.0160	-.0021		
14	14914.5685	-.0019		
15	14914.1057	-.0011		
16	14913.6264	-.0010		
17	14913.1331	.0009		
18	14912.6195	-.0017		
19	14912.0916	-.0028		
20	14911.5495	-.0023	14920.7816	-.0025
21	14910.9914	-.0020	14920.6727	-.0033
22	14910.4211	.0017	14920.5499	-.0022
23	14909.8299	.0004	14920.4128	.0003
24	14909.2232	-.0008	14920.2550	-.0021
25	14908.6030	.0002	14920.0886	.0025
26	14907.9673	.0013	14919.8989	-.0004
27	14907.3140	.0006	14919.6993	.0024
28	14906.6458	.0005	14919.4818	.0030
29	14905.9607	-.0008	14919.2469	.0018
30	14905.2669	.0047	14918.9975	.0017
31	14904.5506	.0033	14918.7307	-.0002
32	14903.8167	-.0001	14918.4527	.0023
33	14903.0692	-.0016	14918.1554	.0011
34	14902.3106	.0012	14917.8379	-.0049
35	14901.5342	.0018	14917.5160	.0003
36	14900.7390	-.0011	14917.1723	-.0009
37	14899.9279	-.0044	14916.8116	-.0036
38	14899.1073	-.0018		
39	14898.2659	-.0047		

Table If. The Observed Line Positions for SrS $A^1\Sigma^+ - X^1\Sigma^+$ (in cm^{-1}).

3-2 Band

J"	P(J")	$\Delta\nu$[a]	R(J")	$\Delta\nu$
2			14151.1791	-.0012
3			14151.3625	-.0010
4	14149.5079	.0021	14151.5360	.0033
5	14149.2137	.0030	14151.6894	.0015
6	14148.9040	.0025	14151.8295	.0003
7	14148.5768	-.0016	14151.9596	.0032
8	14148.2437	.0025		
9	14147.8892	-.0010		
10	14147.5237	-.0014		
11	14147.1440	-.0021		
20			14152.3372	-.0039
21	14142.5897	-.0011	14152.2730	-.0003
22	14142.0565	-.0025	14152.1896	-.0022
23	14141.5120	-.0014	14152.0930	-.0034
24			14151.9836	-.0036
25	14140.3825	.0016	14151.8631	-.0011
26	14139.7952	.0011	14151.7307	.0033
27	14139.1940	.0005	14151.5778	.0009
28	14138.5789	-.0002	14151.4098	-.0029
29	14137.9533	.0022	14151.2331	-.0016
30	14137.3161	.0067	14151.0434	.0004
31	14136.6571	.0030	14150.8356	-.0021
32	14135.9870	.0018	14150.6202	.0015
33	14135.3049	.0023	14150.3858	-.0003
34	14134.6095	.0030	14150.1413	.0014
35	14133.8964	-.0004	14149.8814	.0012
36	14133.1697	-.0040	14149.6093	.0025
37	14132.4360	-.0010		
38	14131.6819	-.0049		

[a] Observed-Calculated line positions using the constants of Table III.

Table Ig. The Observed Line Positions for SrS $A^1\Sigma^+ - X^1\Sigma^+$ (in cm^{-1}).

4-1 Band

J"	P(J")	$\Delta\nu$[a]	R(J")	$\Delta\nu$
1	14868.0878	.0012	14868.7603	.0002
2	14867.8299	-.0008	14868.9567	.0035
3	14867.5590	-.0002	14869.1283	-.0024
4	14867.2682	-.0038	14869.2904	-.0021
5	14866.9644	-.0048	14869.4404	.0018
6	14866.6474	-.0032	14869.5683	-.0008
7	14866.3190	.0025		
8	14865.9719	.0053	14869.7823	-.0007
9	14865.6027	.0016	14869.8623	-.0041
10	14865.2184	-.0016		
11	14864.8220	-.0012		
12	14864.4144	.0036		
13	14863.9827	.0000		
14	14863.5404	.0015		
15	14863.0801	.0005		
16	14862.6045	-.0000		
17	14862.1121	-.0017		
18	14861.6077	.0002		
19	14861.0862	.0008	14869.8390	.0010
20	14860.5488	.0012	14869.7490	.0005
21	14859.9962	.0020		
22	14859.4252	.0003	14869.5234	.0013
23	14858.8414	.0015	14869.3852	.0002
24	14858.2364	-.0026	14869.2329	.0010
25	14857.6250	.0028	14869.0619	-.0008
26	14856.9864	-.0031	14868.8788	.0014
27	14856.3351	-.0057	14868.6759	.0000
28	14855.6751	-.0009	14868.4589	.0009
29	14854.9919	-.0031	14868.2230	-.0006
30	14854.2954	-.0023	14867.9749	.0022
31			14867.7061	.0010
32			14867.4213	.0008
33			14867.1200	.0010
34			14866.8001	-.0001
35			14866.4630	-.0009
36			14866.1136	.0036
37			14865.3480	-.0002
38			14864.9378	-.0019

[a] Observed-Calculated line positions using the constants of Table III.

Table Ih. The Observed Line Positions for SrS $A^1\Sigma^+$ - $X^1\Sigma^+$ (in cm^{-1}).

5-1 Band

J"	P(J")	$\Delta\nu$[a]	R(J")	$\Delta\nu$
2			15204.1716	.0137
3			15204.3349	.0102
4			15204.4830	.0096
5			15204.6119	.0081
6	15201.8427	.0112	15204.7186	.0025
7	15201.4918	.0102	15204.8152	.0048
8	15201.1209	.0072	15204.8887	.0019
9	15200.7335	.0058		
10	15200.3254	.0016		
11	15199.9027	.0007		
12	15199.4618	-.0008		
14	15198.5310	.0001		
15	15198.0341	-.0049	15204.9188	-.0088
16	15197.5243	-.0056	15204.8583	-.0062
17	15196.9967	-.0069	15204.7773	-.0072
18	15196.4537	-.0068	15204.6903	.0024
19	15195.8970	-.0035	15204.5685	-.0062
20	15195.3196	-.0044	15204.4405	-.0046
21	15194.7254	-.0055	15204.2956	-.0036
22	15194.1163	-.0052	15204.1367	-.0006
23	15193.4938	-.0020	15203.9593	-.0000
24	15192.8556	.0015	15203.7685	.0030
25	15192.1962	-.0003	15203.5576	.0016
26	15191.5249	.0018	15203.3327	.0019
27	15190.8382	.0042	15203.0917	.0017
28	15190.1344	.0051	15202.8348	.0010
29	15189.4141	.0049	15202.5584	-.0039
30	15188.6764	.0028	15202.1936	-.0817
31	15187.9232	.0004	15201.9975	.0244
32	15187.0781	-.0785	15201.6677	.0122
33	15186.3940	.0188	15201.3321	.0095
34	15185.5925	.0139	15200.9808	.0065
35	15184.7798	.0131	15200.6158	.0053
36	15183.9473	.0078	15200.2337	.0025
37	15183.1028	.0059	15199.8369	.0008
38	15182.2450	.0062	15199.4231	-.0021
39	15181.3659	.0008		
40	15180.4753	-.0004	15198.5477	-.0071

[a] Observed-Calculated line positions using the constants of Table III.

Table Ih. The Observed Line Positions for SrS $A^1\Sigma^+ - X^1\Sigma^+$ (in cm^{-1}).

5-1 Band (cont.)

J"	P(J")	$\Delta\nu$[a]	R(J")	$\Delta\nu$
41	15179.5715	.0013	15198.0890	-.0058
42	15178.6452	-.0032	15197.6149	-.0029
43	15177.7059	-.0042	15197.1177	-.0056
44	15176.7519	-.0030	15196.6074	-.0036
45	15175.7795	-.0029		
46	15174.7887	-.0035		
47	15173.7846	.0009		
48	15172.7640	.0076		
49	15171.7196	.0100		
50	15170.6539	.0112		

[a] Observed-Calculated line positions using the constants of Table III.

Table Ii. The Observed Line Positions for SrS $A^1\Sigma^+ - X^1\Sigma^+$ (in cm^{-1}).

5-2 Band

J"	P(J")	$\Delta\nu$[a]	R(J")	$\Delta\nu$
9	14817.6340	.0066		
10	14817.2376	.0045		
11	14816.8247	.0027		
12	14816.3978	.0036		
13	14815.9478	-.0019		
14	14815.4866	-.0021		
15	14815.0050	-.0062	14821.8983	-.0016
16	14814.5131	-.0045	14821.8466	-.0056
17	14813.9992	-.0086	14821.7846	-.0041
18	14813.4750	-.0071	14821.7039	-.0056
19	14812.9334	-.0071	14821.6089	-.0058
20	14812.3776	-.0057	14821.4992	-.0052
21	14811.8041	-.0064	14821.3779	-.0010
22	14811.2197	-.0027	14821.2381	-.0001
23	14810.6224	.0034		
24	14810.0014	.0009	14820.9129	.0010
25	14809.3681	.0010	14820.7295	.0030
26	14808.7204	.0016	14820.5301	.0036
27	14808.0601	.0043	14820.3138	.0020
28	14807.3848	.0066	14820.0869	.0042
29	14806.6920	.0059	14819.8404	.0012
30	14805.9858	.0063	14819.5034	-.0778
31	14805.2634	.0048	14819.3243	.0154
32	14804.4478	-.0756	14819.0381	.0158
33	14803.7902	.0164	14818.7287	.0075
34	14803.0243	.0143	14818.4076	.0019
35	14802.2448	.0129		
36	14801.4501	.0106	14817.7283	-.0029
37	14800.6397	.0071	14817.3730	.0011
38	14799.8148	.0036	14816.9940	-.0036
39	14798.9740	-.0011	14816.6049	-.0033
40	14798.1213	-.0030	14816.2002	-.0032
41	14797.2609	.0026	14815.7772	-.0058
42	14796.3753	-.0018	14815.3401	-.0063
43	14795.4790	-.0012	14814.8860	-.0074
44	14794.5695	.0021	14814.4214	-.0022
45	14793.6366	-.0017	14813.9350	-.0013
46	14792.6908	-.0016	14813.4349	.0039
47	14791.7322	.0030		

[a] Observed-Calculated line positions using the constants of Table III.

APPENDIX B

VIBRATION-ROTATION SPECTRUM OF BH $X^1\Sigma^+$ BY FOURIER TRANSFORM EMISSION SPECTROSCOPY

by

F.S. Pianalto, L.C. O'Brien, P.C. Keller and P.F. Bernath[a]

Department of Chemistry
University of Arizona
Tucson, Arizona 85721

[a] Alfred P. Sloan Fellow; Camille and Henry Dreyfus Teacher-Scholar.

8 pages

5 tables

1 figure

ABSTRACT

The vibration-rotation emission spectrum of the BH $X^1\Sigma^+$ state was observed with the McMath Fourier transform spectrometer at Kitt Peak. The 1-0, 2-1 and 3-2 bands were observed in a microwave discharge of B_2H_6 in He. Spectroscopic constants of the individual vibrational levels and equilibrium molecular constants were determined. An RKR potential curve was calculated from the equilibrium constants.

INTRODUCTION

The spectrum of the BH molecule was first studied in 1931 by Lochte-Holtgreven and van der Vleugel (1). Two systems of emission bands, the $A^1\Pi$ - $X^1\Sigma$ system near 4330Å and the $b^3\Sigma$ - $a^3\Pi$ system near 3700Å, were observed in this work.

Since then, several additional spectroscopic studies on BH have been undertaken (2-5). The most extensive work was done in the near and vacuum ultraviolet regions of the spectrum by Bauer, Herzberg and Johns (4) and by Johns, Grimm and Porter (5). Additional experimental work on BH includes a measurement of the dipole moments in the $A^1\Pi$ and $X^1\Sigma^+$ states (6), and the measurements of the radiative lifetime in the $A^1\Pi$ state (7-9).

Presented here is the first vibration-rotation spectrum of BH. The spectrum was recorded in emission from a microwave discharge of diborane in helium with a Fourier transform spectrometer.

Since the BH molecule has only six electrons, the system is frequently used to test the accuracy of various *ab initio* theoretical methods. For example, using the *ab initio* CASSCF technique, Jaszunski, Roos and Widmark (10) mapped out the $B^1\Sigma^+$, $A^1\Pi$ and $X^1\Sigma^+$ potential energy curves of BH. Luh and Stwalley (11) combined these potential curves with experimentally-based RKR potential energy turning points to obtain accurate hybrid potential energy curves. Botschwina (12)

calculated many spectroscopic properties for the $X^1\Sigma^+$ state of BH using ab initio (SCEP-CEPA) methods in order to test the adequacy of such methods for use with the HBF^+ molecule. There have been a large number of additional theoretical calculations on BH (13-25) and our list of references is by no means complete.

EXPERIMENTAL

The BH molecule was observed during an attempt to make BH_3. The boron containing molecules were produced in a microwave discharge of a mixture of approximately 1 Torr He and 0.016 Torr diborane (B_2H_6). The mixture was passed through an electrodeless quartz discharge tube and the discharge was driven by a 2450 MHz microwave oscillator. The diborane used in the discharge was prepared by adding sodium borohydride ($NaBH_4$) to heated polyphosphoric acid under vacuum.

The emission from the discharge tube was observed with the McMath Fourier transform spectrometer associated with the National Solar Observatory at Kitt Peak. Four scans were coadded in approximately 30 minutes of integration. The unapodized resolution was set to 0.02 cm^{-1}. InSb detectors and a silicon filter limited the bandpass region to approximately 1800 to 9000 cm^{-1}. The He atomic line at 5346.9261 cm^{-1} was used to calibrate the wavenumber scale with an absolute accuracy of about $\pm$ 0.002 cm^{-1}. The wavenumber of this line was determined from a previously recorded spectrum which contained both He and Ar.

RESULTS AND DISCUSSION

The interferogram was transformed by G. Ladd to produce the spectrum. The line positions were determined from the spectrum by a data-reduction program, DECOMP, developed at Kitt Peak. The DECOMP program fits the spectral features with Voigt line shape functions to determine the peak positions. Lines with signal-to-noise of less than ~2 were measured by eye. The absolute accuracy and relative precision of the strong unblended lines is estimated to be ± 0.002 cm^{-1}.

Forty-five lines from the vibration-rotation bands 1-0, 2-1, and 3-2 were observed and are listed in Table I. One of the strongest lines in the R-branch is shown in Figure 1. The strongest lines have a signal-to-noise ratio of around 10, while the weakest lines have a ratio of about 1.5. The observed linewidth of the BH lines was approximately 0.025 cm^{-1}. The transitions were assigned with the help of very good spectroscopic constants from the previous high resolution optical study of BH by Johns, Grimm and Porter (5).

The molecular constants of Table II were determined from a nonlinear least-squares fit of all of the transition frequencies given in Table I. The four vibrational levels (v=0-3) were fit simultaneously using the customary $^1\Sigma^+$ energy level expression. The rotational constant H_v for each of the four vibrational levels was held fixed to the values from Johns, Grimm and Porter (5). The molecular constants

determined here agree well with the constants determined by Johns, Grimm and Porter (5), although ours are slightly more accurate.

The lines of Table I were also fit to a $^1\Sigma^+$ Dunham-type (27) energy level expression to determine equilibrium molecular constants presented in Table III.

$$E_{vJ} = \Sigma\, Y_{kl}(v+1/2)^k[J(J+1)]^l$$

The rotational constant H_e was allowed to vary and was determined in this fit. The equilibrium constants of Table III were used to determine a Rydberg-Klein-Rees (RKR) (28) potential curve for the $X^1\Sigma^+$ state. Energies and turning points up to the fourth vibrational level determined from the RKR fit are presented in Table IV. An RKR potential curve for the $^1\Sigma^+$ state of BH was also calculated by Luh and Stwalley (11) using experimental constants of Johns, Grimm and Porter (5). The turning points and rotational constants calculated in the present work agree well with the RKR results determined previously.

Finally, the RKR points and the dissociation energy (D_0=3.42 eV, 30) of BH were input to Hutson's centrifugal distortion program (29) to calculate values of B, D, H and L. The values of these constants for vibrational levels 0-4 are presented in Table V. Hutson's program predicts the experimental constants of Table II with reasonable accuracy. Note that the values for levels v>3 in Tables IV and V are extrapolations and not directly based on observed experimental data.

ACKNOWLEDGMENTS

The National Solar Observatory is operated by the Association for Research in Astronomy, Inc., under contract with the National Science Foundation. We would like to thank J. Wagner and G. Ladd for assistance in acquiring the spectra. This research was supported by the Air Force Astronautics Laboratory, (F 04611-87-K-0020).

REFERENCES (FOR APPENDIX B)

1. W. Lochte-Holtgreven and E.S. van der Vleugel, Z. Physik 70, 188-203 (1931).
2. G.M. Almy and R.B. Horsfall, Phys. Rev., 51, 491-500 (1937).
3. A.E. Douglas, Can. J. Research 19, 27 (1941).
4. S.H. Bauer, G. Herzberg and J.W.C. Johns, J. Mol. Spectrosc. 13, 256-280 (1964).
5. J.W.C. Johns, F.A. Grimm and R.F. Porter, J. Mol. Spectrosc. 22, 435-451 (1967).
6. R. Thomson and F.W. Dalby, Can. J. Phys. 47, 1155-1158 (1969).
7. W.H. Smith, J. Chem. Phys. 54, 1384-1386 (1971).
8. J. Dufayard and O. Nedelec, J. Chem. Phys. 69, 4708-4709 (1978).
9. O. Nedelec and J. Dufayard, J. Chem. Phys. 76, 378-384 (1982).
10. M. Jaszunski, B.O. Roos and P. Widmark, J. Chem. Phys. 75, 306-314 (1981).
11. W. Luh and W.C. Stwalley, J. Mol. Spectrosc. 102, 212-223 (1983).
12. P. Botschwina, J. Mol. Spectrosc. 118, 76-87 (1986).
13. R.M. Stevens and W.N. Lipscomb, J. Chem. Phys. 42, 3666-3669 (1965).
14. J.C. Browne and E.M. Greenawalt, Chem. Phys. Lett. 7, 363-367 (1970).
15. R.J. Harrison and N.C. Handy, Chem. Phys. Lett. 95, 386-391 (1983).

16. R. Cimiraglia and M. Persico, J. Mol. Spectrosc. 87, 303-311 (1981).

17. P.G. Burton, P.J. Bruna and S.D. Peyerimhoff, Chem. Phys. Lett. 95, 379-385 (1983).

18. P.K. Pearson, C.F. Bender and H.F. Schaeffer,III, J. Chem. Phys. 55, 5235-5241 (1971).

19. W. Meyer and P. Rosmus, J. Chem. Phys. 63, 2356-2375 (1975).

20. J.A. Pople and P.v.R. Schleyer, Chem. Phys. Lett. 129, 279-281 (1986).

21. J. Noga and R.J. Bartlett, J. Chem. Phys. 86, 7041-7050 (1987).

22. G.H.F. Diercksen, N.E. Gruner, J.R. Sabin and J. Oddershede, Chem. Phys. 115, 15-21 (1987).

23. A.V. Nemukhin, N.F. Stepanov and V.I. Pupyschev, Chem. Phys. Lett. 115, 241-244 (1985).

24. D.M. Bishop, J. Pipin and B. Lam, Chem. Phys. Lett. 127, 377-380 (1986).

25. G. Maroulis and D.M. Bishop, Chem. Phys. 96, 409-418 (1985).

26. G. Herzberg, Spectra of Diatomic Molecules, 2nd edition, Van Nostrand, New York, 1950.

27. J.L. Dunham, Phys. Rev. 41, 721-731 (1932).

28. H. Lefebvre-Brion and R.W. Field, Perturbations in the Spectra of Diatomic Molecules, Academic Press, Orlando, FL, 1986, pg. 189-192.

29. J. Hutson, J. Phys. B, 14 851-857 (1981).

30. K.P. Huber and G. Herzberg, Constants of Diatomic Molecules, Van Nostrand Reinhold, New York, 1979.

Table I. The Observed Line Positions for the Vibration-Rotation Spectrum of BH $X^1\Sigma^+$ (in cm^{-1}).

J"	P(J")	$\Delta\nu$[a]	R(J")	$\Delta\nu$
		1-0 Band		
0	-		2292.0226	-0.0010
1	2245.6007	0.0006	2313.9611	-0.0010
2	2221.1747	0.0014	2335.0148	0.0009
3	2195.9750	-0.0009	2355.1511	-0.0003
4	2170.0391	0.0009	2374.3478	-0.0002
5	2143.3900	-0.0006	2392.5762	-0.0013
6	2116.0647	0.0011	2409.8158	0.0009
7	2088.0859	-0.0021	2426.0366	0.0004
8	2059.4945	0.0000	2441.2194	0.0012
9	2030.3159	0.0023	2455.3379	-0.0010
		2-1 Band		
0	-		2195.7896	0.0015
1	2151.0131	0.0024	2216.9235	-0.0004
2	2127.4232	-0.0030	2237.1874	0.0001
3	2103.0828	-0.0005	2256.5511	-0.0003
4	2078.0125	0.0007	2274.9894	-0.0005
5	2052.2411	-0.0006	2292.4752	-0.0021
6	2025.8035	0.0005	2308.9905	0.0017
7	1998.7280	0.0020	2324.4993	-0.0012
		3-2 Band		
2	-		2141.5784	0.0019
3	2012.3338	0.0014	2160.1684	-0.0064
4	1988.1081	-0.0003	2177.8702	0.0062
5	1963.1988	0.0021	2194.6328	0.0118
6	1937.6215	-0.0069	2210.4280	0.0043
7	1911.4273	-0.0079	2225.2492	-0.0022

[a] Observed - Calculated line positions using the constants of of Table II.

Table II. Molecular Constants for BH $X^1\Sigma^+$ (cm^{-1}).

Constant	v=0	v=1	v=2	v=3
T_v	0.0	2269.22670(53)	4443.0344(11)	6523.6106(75)
B_v	11.815729(55)	11.400868(45)	10.992600(86)	10.58980(48)
$D_v \times 10^3$	1.22371(58)	1.20196(39)	1.1786(11)	1.1418(61)
$H_v \times 10^7$	1.125[a]	1.097[a]	0.91[a]	0.90[a]

[a] Held fixed to values of Johns, Grimm and Porter (Ref. 5).

Table III. Equilibrium Molecular Constants for BH $X^1\Sigma^+$ (cm^{-1}).

Constant[a]	Value
ω_e	2366.7275(28)
$\omega_e x_e$	49.3384(20)
$\omega_e y_e$	0.36194(42)
B_e	12.025542(77)
α_e	0.421516(46)
γ_e	0.003317(13)
$D_e \times 10^3$	1.2313(14)
$\beta_e \times 10^5$	-2.190(40)
$H_e \times 10^7$	0.873(99)
r_e (Å)	1.232179(3)

[a] As defined in Ref. 26, pg. 92, 107 and 108.

Table IV. RKR Turning Points for BH $X^1\Sigma^+$.

v	E_v (cm^{-1})	R_{min} (Å)	R_{max} (Å)
0.0	1172.6335	1.12036	1.37113
0.5	2319.3101	1.08069	1.43834
1.0	3441.8604	1.05255	1.49444
1.5	4540.5558	1.03030	1.54511
2.0	5615.6678	1.01174	1.59253
2.5	6667.4679	0.99579	1.63781
3.0	7696.2274	0.98177	1.68163
3.5	8702.2179	0.96928	1.72442
4.0	9685.7108	0.95801	1.76649

Table V. Rotational Constants Calculated from the Potential Curve of Table IV (in cm^{-1}).

Constant	v=0	v=1	v=2	v=3	v=4
B_v	11.8159	11.4006	10.9924	10.5910	10.1960
$D_v \times 10^3$	1.230	1.207	1.185	1.161	1.138
$H_v \times 10^7$	1.08	1.06	1.04	1.02	1.01
$L_v \times 10^{11}$	-1.3	-1.4	-1.2	-1.3	-1.5

Figure 1. The R(5) line of the fundamental (1-0) vibration-rotation band of BH.

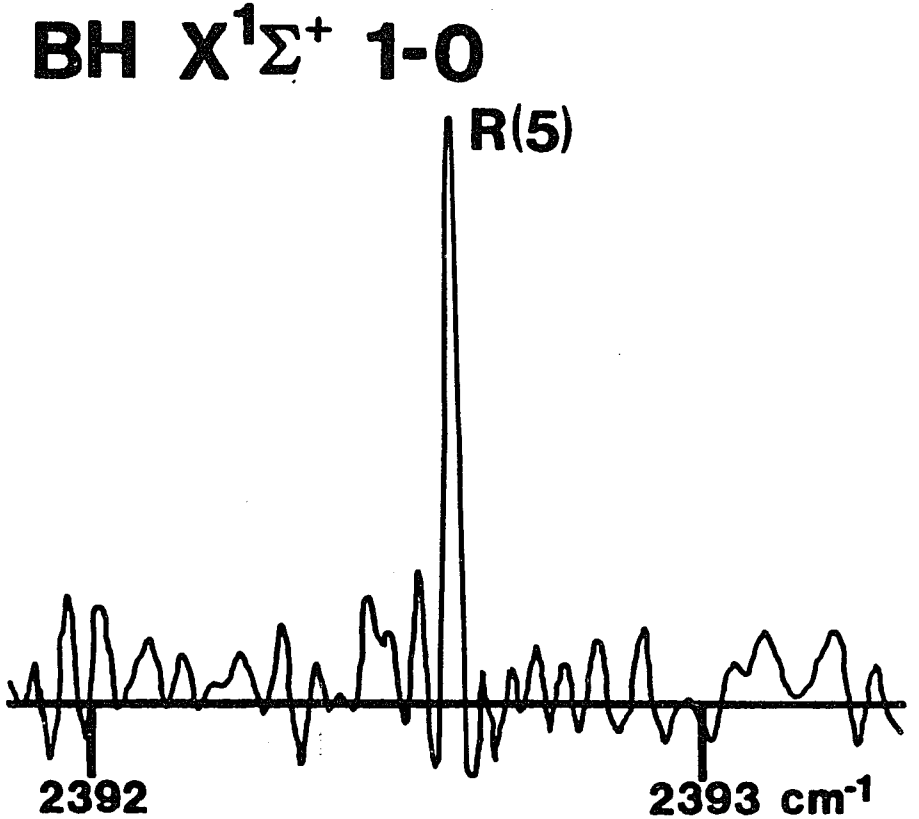
BH $X^1\Sigma^+$ 1-0
R(5)
2392
2393 cm^{-1}

LIST OF REFERENCES

1. J.B. West, R.S. Bradford, J.D. Eversole and C.R. Jones, Rev. Sci. Instrum. 46, 164-168 (1975).

2. L.C. O'Brien, Ph. D. Thesis, University of Arizona 1987.

3. C.R. Brazier and P.F. Bernath, J. Chem. Phys. 86, 5918-5922 (1987).

4. L.C. O'Brien, C.R. Brazier and P.F. Bernath, in press, J. Mol. Spectrosc.

5. C.R. Brazier, L.C. O'Brien, S.M. Kinsey-Nielsen, and P.F. Bernath, in preparation.

6. D.G. Sutton and S.N. Suchard, Appl. Opt. 14, 1898-1910 (1975).

7. M. Farber and R.D. Srivastava, High Temp. Sci. 7, 74-80 (1975).

8. K. Schofield and T.M. Sugden, 10, 1965 Symp. (Int.) Combust., 589-604 (1965).

9. D.E. Jensen and G.A. Jones, Proc. R. Soc. London A A364, 509-535 (1978).

10. J.W. Hastie, High Temperature Vapors; Science and Technology; Academic Press, New York, 1975.

11. M. Marcano and R.F. Barrow, Trans. Faraday Soc. 66, 1917-1919 (1970).

12. H. Partridge, S.R. Langhoff and C.W. Bauschlicher, Jr., J. Chem. Phys. 88, (1988).

13. F.S. Pianalto, C.R. Brazier, L.C. O'Brien and P.F. Bernath, in preparation.

14. R. Colin, P. Goldfinger and M. Jeunehomme, Trans. Faraday Soc. 60, 306-316 (1964).

15. J.R. Marquart and J. Berkowitz, J. Chem. Phys. 39, 283-285 (1963).

16. E.D. Cater and E.W. Johnson, J. Chem. Phys. 47, 5353-5357 (1967).

17. T.P. Martin and H. Schaber, Spectrochimica Acta 38A, 655-660 (1982).

18. W.J.M. Gissane and R.F. Barrow, Proc. Phys. Soc. 82, 1065-1066 (1963).

19. C.J. Cheetham, W.J.M. Gissane and R.F. Barrow, Trans. Faraday Soc. 61, 1308-1316 (1965).

20. B. Pouilly, J.M. Robbe, J. Schamps, R.W. Field and L. Young, J. Mol. Spectrosc. 96, 1-55 (1982).

21. M. Marcano and R.F. Barrow, Trans. Faraday Soc. 66, 2936-2938 (1970).

22. R.C. Blues and R.F. Barrow, Trans. Faraday Soc. 65, 646-648 (1969).

23. R.F. Barrow, W.J.M. Gissane and G.V.M. Rose, Proc. Phys. Soc. 84, 1035 (1964).

24. R.M. Clements and R.F. Barrow, Chem. Comm. 22, 1408 (1968).

25. R.F. Barrow, W.G. Burton and P.A. Jones, Trans. Faraday Soc. 67, 902-906 (1971).

26. P.G. Cummins, R.W. Field and I. Renhorn, J. Mol. Spectrosc. 90, 327-352 (1981).

27. G. Almkvist and A. Lagerqvist, Arkiv Fysik 1, 477-494 (1949); 2, 233-251 (1950); 8, 481-488 (1954).

28. A. Lagerqvist and L.E. Selin, Arkiv Fysik 11, 323-328 (1956).

29. L. Brewer and R. Hauge, J. Mol. Spectrosc. 25, 330-339 (1968).

30. J.L. Dunham, Phys. Rev. 41, 721-731 (1932).

31. H. Lefebvre-Brion and R.W. Field, Perturbations in the Spectra of Diatomic Molecules, Academic Press, Orlando, FL, 1986, pg. 189-192.

32. K.P. Huber and G. Herzberg, Constants of Diatomic Molecules, Van Nostrand Reinhold, New York, 1979.

33. J. Hutson, J. Phys. B 14, 851-857 (1981).

34. G. Herzberg, Spectra of Diatomic Molecules, 2nd edition, Van Nostrand Reinhold, New York, 1950.

35. M.B. Hall and R.F. Fenske, Inorg. Chem. 11, 768-775 (1972).

36. B.D. James and M.G.H. Wallbridge, Prog. Inorg. Chem. 11, 99-231 (1970).

37. T.J. Marks and J.R. Kolb, Chem. Rev. 77, 263-293 (1977).

38. A. Almenningen, G. Gundersen and A. Haaland, Chem. Commun., 557-559 (1967).

39. A. Almenningen, G. Gundersen and A. Haaland, Acta Chem. Scand. 22, 859-866 (1968).

40. F.S. Pianalto, C.R. Brazier, L.C. O'Brien, P.C. Keller and P.F. Bernath, in preparation.

41. A.I. Boldyrev, O.P. Charkin, N.G. Rambidi and V.I. Avdeev, Chem. Phys Letters 44, 20-24 (1976).

42. A.I. Boldyrev, O.P. Charkin, N.G. Rambidi and V.I. Avdeev, Russian J. Struct. Chem. 18, 16-28 (1977); 19, 203-210 1978.

43. A.I. Boldyrev and O.P. Charkin, Russian J. Struct. Chem. 18, 783 (1987); 20, 969-977 (1977).

44. J.D. Dill, P.v.R. Schleyer, J.S. Binkley and J.A. Pople, J. Am. Chem. Soc. 99, 6159-6173 (1977).

45. B.I. Zhilinski, J. Molec. Struct. 46, 183-188 (1978).

46. R. Bonaccorsi, E. Scrocco and J. Tomasi, Theoret. Chem. Acta (Berl.) 52, 113-117 (1979).

47. V.G. Zakzhevskii, A.I. Boldyrev and O.P. Charkin, Chem. Phys. Letters 73, 54-57 (1980).

48. S. Bhargava and N.K. Ray, Int. J. of Quantum Chem. 17, 907-914 (1980).

49. V. Barane, G. Dolcetti, F. Lelj and N. Russo, Inorg. Chem. 20, 1687-1691 (1981).

50. L.Ya. Baranov and A.I. Boldyrev, Chem. Phys. Letters 96, 218-222 (1983).

51. V. Kello, M. Urban and A.I. Boldyrev, Chem. Phys. Letters 106, 455-459 (1984).

52. L.Ya. Baranov and A.I. Boldyrev, Molec. Phys. 54, 989-998 (1985).

53. D.J. Defrees, K. Raghavachari, H.B. Schlegel and J.A. Pople, J. Phys. Chem. 91, 1857-1864 (1987).

54. A.M.R.P. Bopegedera, F.S. Pianalto, C.R. Brazier and P.F. Bernath, work in progress.